Supporting Information: Acceleration of CO_2 Insertion into Metal Hydrides: Ligand, Lewis Acid, and Solvent Effects on Reaction Kinetics

Jessica E. Heimann,[†] Wesley H. Bernskoetter,[§] Nilay Hazari,[*,†] and James M. Mayer[†]

[†]*The Department of Chemistry, Yale University, P. O. Box 208107, New Haven, Connecticut, 06520, USA.* [§]*The Department of Chemistry, University of Missouri, Columbia, Missouri, 65211, USA.*
E-Mail: nilay.hazari@yale.edu

Table of Contents

Experimental Details

General Methods

Experiments were performed under a dinitrogen atmosphere in a glove box or using standard Schlenk techniques, unless otherwise noted. Moisture- and air-sensitive liquids were transferred by stainless steel cannula on a Schlenk line or in a glove box. All commercial chemicals were used as received, except where noted. THF, benzene, pentane, toluene, diethyl ether, and dichloromethane were dried by passage through a column of activated alumina followed by storage under dinitrogen. Anhydrous carbon dioxide was purchased from Airgas, Inc and used as received. Pyridine was dried over calcium hydride and distilled prior to use. Acetone was purchased from J. T. Baker and degassed prior to use. 1,2-Dichloroethane and triethylamine were purchased from Sigma Aldrich and degassed prior to use. 1,3-Dimethyl-2-imidazolidinone was purchased from EMD Chemicals and degassed prior to use. 1,4-Dioxane was purchased from Acros Organics and distilled prior to use to remove butylated hydroxytoluene (BHT). Glyme (1,2-dimethoxyethane) was purchased from Acros Organics and dried over molecular sieves prior to use. Diglyme (diethylene glycol dimethyl ether) was purchased from Sigma Aldrich and dried over molecular sieves prior to use. Methanol was purchased from MilliporeSigma and degassed prior to use. Ethanol was purchased from Decon Labs and degassed prior to use. Sodium trifluoromethanesulfonate, sodium trifluoromethanesulfonimide, lithium trifluoromethanesulfonimide, lithium hexafluorophosphate, and sodium tetraphenylborate were purchased from Sigma Aldrich and dried overnight at 40 °C under vacuum prior to use. Lithium tetraphenylborate tris dimethoxyethane was purchased from Santa Cruz Biotechnology and dried overnight at 40 °C under vacuum prior to use. Lithium trifluoromethanesulfonate and potassium trifluoromethanesulfonimide were purchased from Strem Chemicals and dried overnight at 40 °C under vacuum prior to use. Sodium tetrakis[3,5-bis(trifluoromethyl)phenyl]borate was purchased from Alfa Aesar and dried overnight at 40 °C under vacuum prior to use. Tetrabutylammonium hexafluorophosphate was purchased from Sigma Aldrich and recrystallized from ethanol three times prior to use. Acetonitrile was purchased from Honeywell Burdick & Jackson and used as received. *n*-Hexane, carbon tetrachloride, pinacolborane, silver acetate, and sodium borohydride were purchased from Acros Organics and used as received. Di-*tert*-butylphosphine was purchased from Strem Chemicals and used as received. 1,3-Dimethyl-5-iodobenzene and nickel(II) chloride hexahydrate were purchased from Alfa Aesar and used as received. *N*-

bromosuccinimide and benzoyl peroxide were purchased from Sigma Aldrich and used as received. Potassium tetrakis(pentafluorophenyl)borate was purchased from Boulder Scientific Company and used as received. Sodium borodeuteride was purchased from Cambridge Isotope Laboratories. Literature procedures were used to prepare (^{tBu}PCP)NiH (**1**),[1] (^{Cy}PCP)NiH (**2**),[1] (^{iPr}PCP)NiH (**3**),[1] 1,3-di(bromomethyl)-5-anisole,[2] and (^{iPr}PN^{H}P)IrH$_3$ (**6**).[3] C_6D_6 was dried by passing through activated alumina followed by storage under dinitrogen. CH_3CH_2OD was degassed prior to use. NMR spectra were recorded on Bruker AMX-400, AMX-500, or AMX-600 spectrometers at ambient probe temperatures. Chemical shifts are reported in ppm with respect to residual internal protio solvent for ^{1}H NMR spectra. High-resolution mass spectrometry experiments were performed by the School of Chemical Sciences Mass Spectrometry Laboratory at the University of Illinois Urbana-Champaign. Robertson Microlit Laboratories, Inc. performed the elemental analyses (inert atmosphere).

Synthesis and Characterization of New Compounds

Synthesis of (^{R}PCP)Ni{OC(O)H} Complexes

(^{iPr}PCP)Ni{OC(O)H} (**3-CO_2**)

(^{iPr}PCP)NiH (**3**) (15 mg, 0.038 mmol) was dissolved in 600 μL C_6D_6 and added to a J Young tube. The nitrogen atmosphere was evacuated, and an excess of 1 atm CO_2 was added via a Schlenk line at room temperature. After 10 min, the solvent was removed to give **3-CO_2** as a yellow solid. The product was recrystallized from pentane at -30 °C. Yield: 16 mg (96 %).

^{1}H NMR (C_6D_6, 500.0 MHz): 8.54 (s, 1H, NiOC(O)*H*), 7.00 (t, 1H, Ar*H*, J = 7.4 Hz), 6.82 (d, 2H, Ar*H*, J = 7.4 Hz), 2.69 (vt, 4H, ArCH_2P, J = 3.8 Hz), 1.96 (m, 4H, PC*H*$(CH_3)_2$) 1.40 (dvt, 12H, PCH(CH_3)$_2$, $^{3}J_{HH}$ = 8.3 Hz, J*$_{HP}$ = 23.1 Hz), 0.99 (dvt, 12H, PCH(CH_3)$_2$, $^{3}J_{HH}$ = 6.8 Hz, J*$_{HP}$ = 20.7 Hz). ^{13}C{^{1}H} NMR (C_6D_6, 125.7 MHz): 167.2 (s, NiO*C*(O)H), 152.9 (t, J = 13.1 Hz), 125.4 (s), 122.4 (t, J = 8.71 Hz), 31.5 (t, J = 13.28 Hz), 24.1 (t, J = 9.92 Hz), 19.0 (vt, J = 2.3z Hz), 18.1 (s). ^{31}P{^{1}H} NMR (C_6D_6, 202.4 MHz): 57.96. IR (Diamond ATR cell, cm^{-1}): 1617.2 (CO_2), 1316.3 (CO_2). Anal found (calcd for $C_{21}H_{36}P_2O_2Ni$): C 57.12 (57.17), H 7.95 (8.23) %.

Synthesis of (p-OMe-^{tBu}PCP)Ni Complexes

(*p*-OMe-^{tBu}PCP)H

(*p*-OMe-^{tBu}PCP)H was synthesized by a modification of a related literature procedure.[4] A slurry of 1,3-di(bromomethyl)-5-anisole (480 mg, 1.6 mmol) in MeOH was prepared in a Schlenk flask. $^{t}Bu_2PH$ (525 mg, 3.6 mmol) was then added and the mixture stirred for 48 h. During this time, the solution became homogeneous. After 48 h, NEt_3 (496 mg, 0.68 mL, 4.9 mmol) was added to the stirring solution via syringe. The solution was left to stir for 2 h, and then the solvent was removed under vacuum. The desired product was extracted into pentane and filtered. Removing the pentane under vacuum left the desired product as an oil. Yield: 600 mg (88 %). The ^{1}H and ^{31}P NMR spectra of this compound matched that previously reported in the literature.[2]

(*p*-OMe-^{tBu}PCP)NiCl

(*p*-OMe-^{tBu}PCP)NiCl was synthesized by a modification of the known literature procedure for the preparation of (^{tBu}PCP)NiCl.[1] $NiCl_2{\cdot}(H_2O)_6$ (336 mg, 1.4 mmol) was dissolved in degassed water (1 mL) and added to a flask charged with (*p*-OMe-^{tBu}PCP)H (600 mg, 1.4 mmol) in

ethanol (8 mL). The solution was heated at reflux for 24 h. Within the first two hours of reflux, the solution turned bright yellow. The solution was then cooled to room temperature and concentrated. The precipitate was collected by filtration and the desired product extracted in pentane and filtered again. The pentane was finally removed under vacuum, leaving the desired product as a golden yellow solid. Yield: 332 mg (45 %).

^{1}H NMR (C_6D_6, 500.0 MHz): 6.56 (s, 2H, Ar*H*), 3.49 (s, 3H, ArOC*H*$_3$), 2.87 (s, 4H, ArC*H*$_2$P), 1.43 (t, 36H, PC(C*H*$_3$)$_3$, J = 6.3 Hz). ^{13}C{^{1}H} NMR (C_6D_6, 150.8 MHz): 158.8 (t, J = 1.9 Hz), 153.8 (t, J = 13.1 Hz), 144.9 (t, J = 17.4 Hz), 108.1 (t, J = 8.7 Hz), 54.7 (s, ArO*C*H$_3$), 34.8 (t, J = 6.8 Hz), 34.3 (t, J = 11.6 Hz), 29.8 (t, J = 2.2 Hz). ^{31}P{^{1}H} NMR (C_6D_6, 202.4 MHz): 66.25. HRMS (EI^{+}): 516.1991 [M]$^{+}$. Calcd. for [$C_{25}H_{45}OP_2ClNi$]: 516.1988.

(*p*-OMe-^{tBu}PCP)NiH (**4**)

(*p*-OMe-^{tBu}PCP)NiH was synthesized by a modification of the known literature procedure for the preparation of (^{tBu}PCP)NiH (**1**).[1] $NaBH_4$ (91.3 mg, 2.4 mmol) and ethanol (8 mL) were added to a flask charged with (*p*-OMe-^{tBu}PCP)NiCl (125 mg, 0.24 mmol) in benzene (8 mL). The solution was stirred at 40 °C for 24 h, and then an additional 250 mg $NaBH_4$ was added. The reaction continued stirring at 40 °C for 20 h, after which the reaction was cooled to room temperature and the solvent removed. The product was extracted into benzene (15 mL) and filtered. The benzene was removed under vacuum to give **4** as a yellow solid. The desired product was recrystallized from pentane at -35 °C. Yield: 112 mg (96 %).

^{1}H NMR (C_6D_6, 400.0 MHz): 6.92 (s, 2H, Ar*H*), 3.61 (s, 3H, ArOC*H*$_3$), 3.27 (s, 4H, ArC*H*$_2$P), 1.28 (t, 36H, PC(C*H*$_3$)$_3$, J = 6.4 Hz), -10.08 (t, 1H, Ni*H*, J = 52.8 Hz). ^{13}C{^{1}H} NMR (C_6D_6, 150.8 MHz): 169.4 (m), 158.8 (t, J = 1.7 Hz), 153.6 (t, J = 13.8 Hz), 107.5 (t, J = 8.7 Hz), 54.8 (s, ArO*C*H$_3$), 38.1 (t, J = 11.5 Hz), 33.6 (t, J = 8.1 Hz), 29.8 (t, J = 3.0 Hz). ^{31}P{^{1}H} NMR (C_6D_6, 161.9 MHz): 100.41. Anal found (calcd for $C_{25}H_{46}OP_2Ni$): C 62.15 (62.13), H 9.44 (9.59) %.

(*p*-OMe-^{tBu}PCP)Ni{OC(O)H} (**4-CO$_2$**)

(*p*-OMe-^{tBu}PCP)NiH (**4**) (30 mg, 0.062 mmol) was dissolved in 600 µL C_6D_6 and added to a J Young tube. The nitrogen atmosphere was evacuated, and an excess of 1 atm CO_2 was added via a Schlenk line at room temperature. Under 1 atm CO_2, **4-CO$_2$** was formed in quantitative yield. Attempts to cleanly isolate **4-CO$_2$**, however, were unsuccessful, as it was found to partially

decarboxylate under vacuum resulting in the reformation of a small amount of compound **4**. The ^{1}H, ^{31}P, and ^{13}C NMR spectra provided below (Figures S1-S3) were obtained under 1 atm CO_2.

^{1}H NMR (C_6D_6, 500.0 MHz): 8.64 (s, 1H, NiOC(O)*H*), 6.49 (s, 2H, Ar*H*), 3.47 (s, 3H, ArOC*H*$_3$), 2.81 (s, 4H, ArC*H*$_2$P), 1.35 (t, 36H, PC(C*H*$_3$)$_3$, J = 6.3 Hz). $^{13}C\{^{1}H\}$ NMR (C_6D_6, 100.6 MHz): 168.2 (s, NiO*C*(O)H), 159.0 (t, J = 1.9 Hz), 153.7 (t, J = 12.4 Hz), 139.2 (t, J = 18.1 Hz), 108.3 (t, J = 8.5 Hz), 54.7 (s, ArO*C*H$_3$), 34.4 (t, J = 6.1 Hz), 33.5 (t, J = 12.5 Hz), 29.6 (t, J = 2.5 Hz). $^{31}P\{^{1}H\}$ NMR (C_6D_6, 202.4 MHz): 66.96. IR (Diamond ATR cell, cm^{-1}): 1626.2 (CO_2), 1318.9 (CO_2). Elemental analysis was not obtained for compound **4-CO$_2$**, as it was found to partially decarboxylate under vacuum.

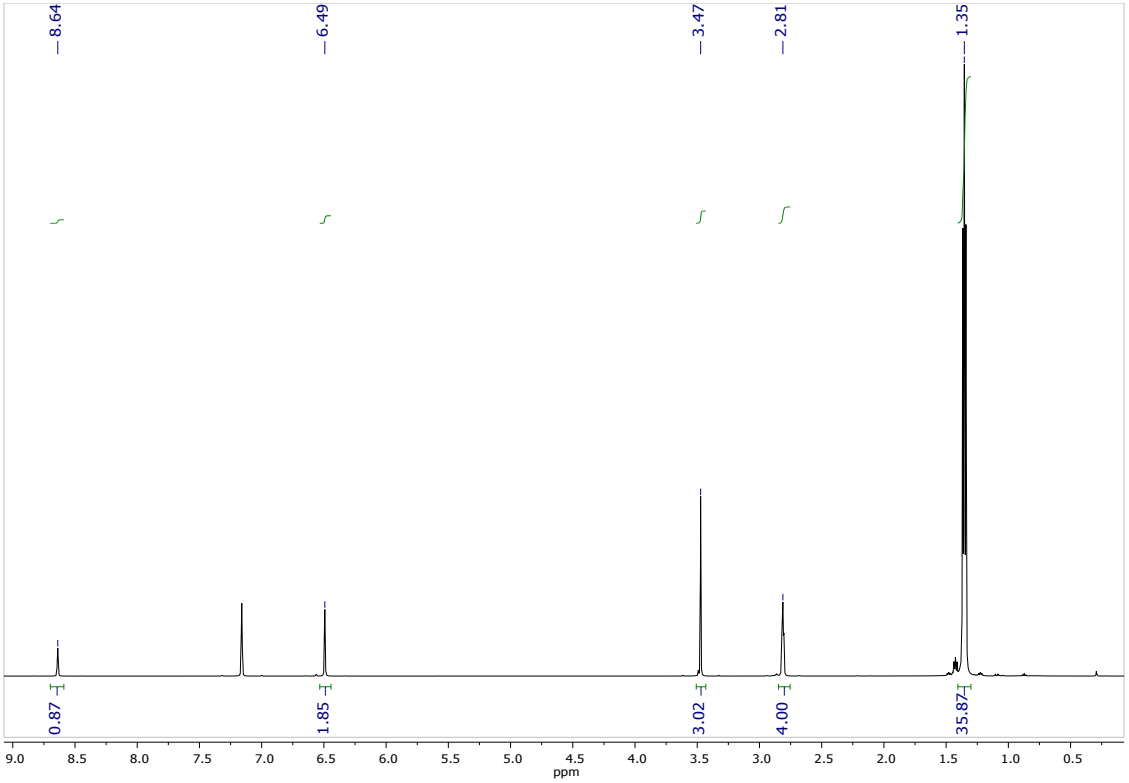

Figure S1: ^{1}H NMR spectrum of **4-CO$_2$** in C_6D_6 under 1 atm CO_2.

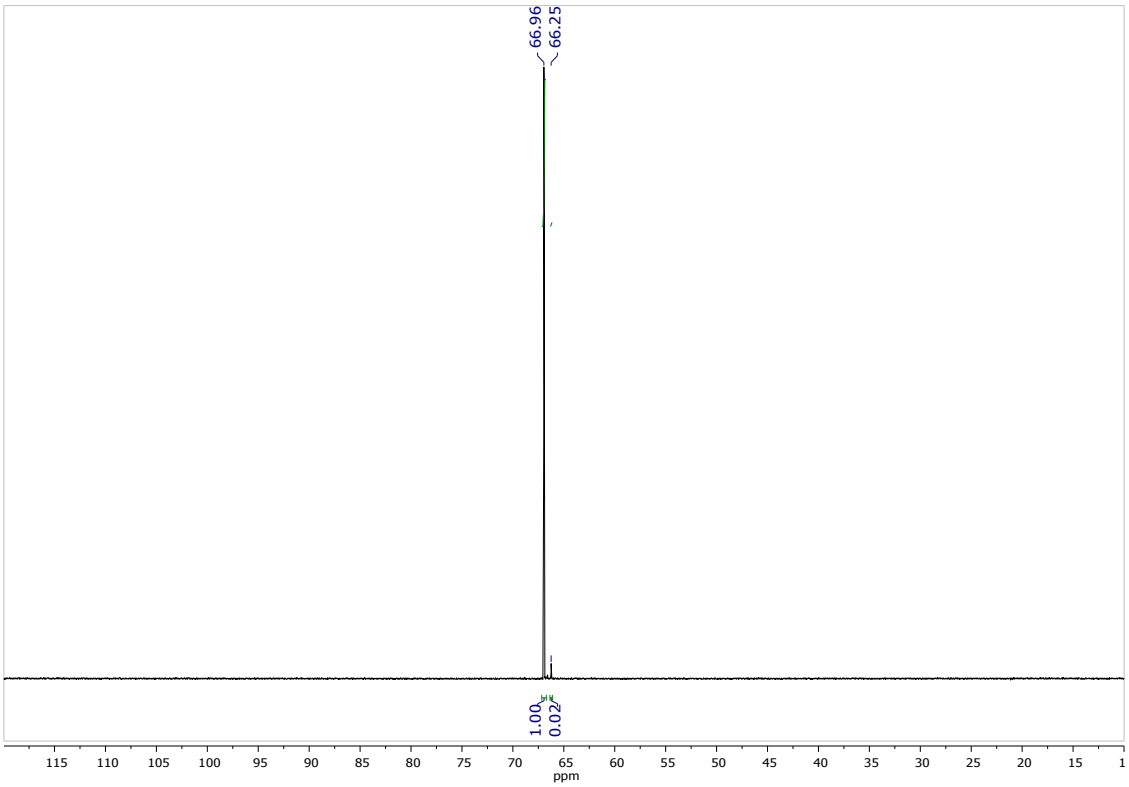

Figure S2: ^{31}P NMR spectrum of **4-CO_2** in C_6D_6 under 1 atm CO_2. The peak at 66.25 ppm is residual (*p*-OMe-^{tBu}PCP)NiCl.

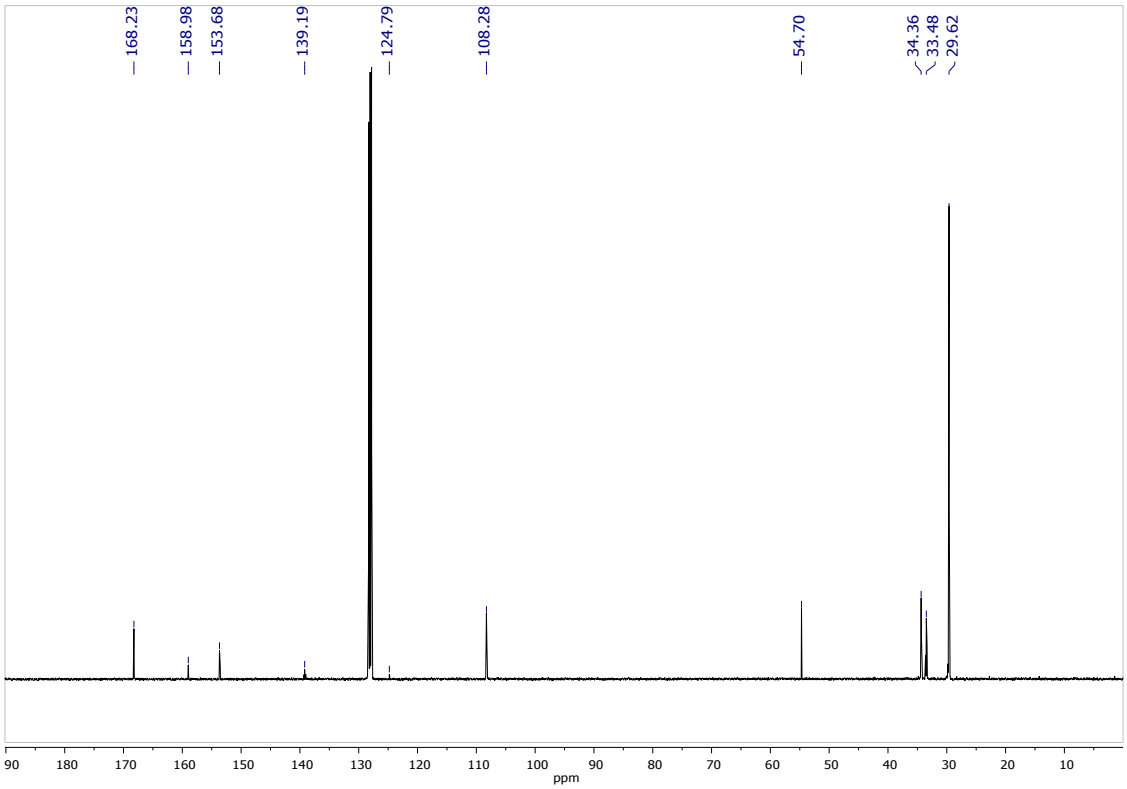

Figure S3: $^{13}C\{^1H\}$ NMR spectrum of **4-CO_2** in C_6D_6 under 1 atm CO_2. The peak at 124.8 ppm is free CO_2.

Synthesis of (p-I-^{tBu}PCP)Ni Complexes

1,3-Di(bromomethyl)-5-iodobenzene

1,3-Di(bromomethyl)-5-iodobenzene was synthesized by a modification of the known literature procedure for 1,3-di(bromomethyl)-5-anisole.[2] A mixture of 1,3-dimethyl-5-iodobenzene (2.85 g, 12.3 mmol), *N*-bromosuccinimide (4.57 g, 25.7 mmol), and benzoyl peroxide (50 mg, 0.2 mmol) in carbon tetrachloride (25 mL) were heated at reflux for 16 h. The solution was then cooled to room temperature and the solid succinimide removed by filtration. The solvent was removed from the filtrate under vacuum, leaving a dark purple/red oil. The desired product was obtained as a white solid through successive recrystallizations, one from dichloromethane followed by two from toluene/pentane. Yield: 823 mg (17 %). The ^{1}H NMR spectrum of this compound matched that previously reported in the literature.[5]

(*p*-I-^{tBu}PCP)H

(*p*-I-^{tBu}PCP)H was synthesized by a modification of a related literature procedure.[4] A slurry of 1,3-di(bromomethyl)-5-iodobenzene (820 mg, 2.1 mmol) in MeOH was prepared in a Schlenk flask. $^{t}Bu_2PH$ (679 mg, 4.6 mmol) was then added and the mixture stirred for 48 h. During this time, the solution became homogeneous. After 48 h, NEt_3 (850 mg, 1.17 mL, 8.4 mmol) was added to the stirring solution via syringe. The solution continued stirring for 3 h, and then the solvent was removed under vacuum. The desired product was extracted into pentane and filtered. Removing the pentane under vacuum left the desired product as a white solid. Yield: 652 mg (60 %).

^{1}H NMR (C_6D_6, 400.0 MHz): 7.74 (s, 2H, Ar*H*), 7.54 (s, 1H, Ar*H*), 2.58 (s, 4H, ArCH_2P), 1.01 (d, 36H, PC(CH_3)$_3$, J = 10.7 Hz). ^{13}C{^{1}H} NMR (C_6D_6, 100.6 MHz): 144.6 (d, J = 13.0 Hz), 136.2 (d, J = 9.3 Hz), 131.0 (t, J = Hz), 94.7 (s), 31.8 (d, J = 24.1 Hz), 29.9 (d, J = 13.6 Hz), 28.6 (d, J = 26.3 Hz). ^{31}P{^{1}H} NMR (C_6D_6, 161.9 MHz): 33.56. HRMS (EI^{+}): 521.1984 [M+H]$^{+}$. Calcd. for [$C_{24}H_{44}P_2I$]: 521.1963.

(*p*-I-^{tBu}PCP)NiCl

(*p*-I-^{tBu}PCP)NiCl was synthesized by a modification of the known literature procedure for the preparation of (^{tBu}PCP)NiCl.[1] $NiCl_2{\cdot}(H_2O)_6$ (251 mg, 1.06 mmol) was dissolved in degassed water (2 mL) and added to a flask charged with (*p*-I-^{tBu}PCP)H (550 mg, 1.06 mmol) in ethanol (10 mL). The solution was heated at reflux for 48 h. Within the first two hours of reflux, the

solution turned bright yellow. The solution was then cooled to room temperature and concentrated. The precipitate was collected by filtration and the desired product extracted in pentane and filtered again. The pentane was finally removed under vacuum, leaving the desired product as a golden yellow solid. Yield: 332 mg (51 %).

^{1}H NMR (C_6D_6, 400.0 MHz): 7.12 (s, 2H, Ar*H*), 2.65 (vt, 4H, ArCH_2P, J = 3.6 Hz), 1.34 (t, 36H, PC(CH_3)$_3$, J = 6.5 Hz). ^{13}C{^{1}H} NMR (C_6D_6, 125.7 MHz): 155.7 (t, J = 16.7 Hz), 155.3 (t, J = 13.0 Hz), 130.5 (t, J = 8.4 Hz), 90.6 (s), 34.9 (t, J = 6.8 Hz), 33.7 (t, J = 11.4 Hz), 29.7 (t, J = 2.1 Hz). ^{31}P{^{1}H} NMR (C_6D_6, 161.9 MHz): 66.45. HRMS (EI$^+$): 577.1179 [M-Cl]$^+$. Calcd. for [$C_{24}H_{42}P_2NiI$]: 577.1160.

(*p*-I-^{tBu}PCP)Ni{OC(O)CH$_3$}

(*p*-I-^{tBu}PCP)Ni{OC(O)CH$_3$} was synthesized by a modification of the known literature procedure for (^{tBu}PCP)Ni{OC(O)CH$_3$}.[6] A solution of (*p*-I-^{tBu}PCP)NiCl (200 mg, 0.3 mmol) in THF (4 mL) was added to a flask charged with silver acetate (274 mg, 1.6 mmol). The mixture was heated at 50 °C for 132 h and then cooled to room temperature. The solvent was removed under vacuum and the product extracted into pentane and filtered. The pentane was removed under vacuum to give a yellow residue. The residue was dissolved in benzene and loaded on a short silica column. The column was first washed with benzene to remove an impurity (yellow band). The desired product was then eluted as the second band (golden yellow) with 1:1 ether/benzene. Removal of the solvent gave the desired product as a yellow solid. Yield: 167 mg (80 %).

^{1}H NMR (C_6D_6, 400.0 MHz): 7.06 (s, 2H, Ar*H*), 2.62 (vt, 4H, ArCH_2P, J = 3.6 Hz), 2.06 (s, 3H, NiOC(O)CH_3), 1.29 (t, 36H, PC(CH_3)$_3$, J = 6.5 Hz). ^{13}C{^{1}H} NMR (C_6D_6, 125.7 MHz): 175.4 (s, NiO*C*(O)CH$_3$), 155.3 (t, J = 12.4 Hz), 1551.2 (t, J = 17.5 Hz), 130.5 (t, J = 8.1 Hz), 90.6 (s), 34.3 (t, J = 6.1 Hz), 33.0 (t, J = 12.1 Hz), 29.4 (t, J = 2.5 Hz), 25.9 (s, NiOC(O)*C*H$_3$). ^{31}P{^{1}H} NMR (C_6D_6, 161.9 MHz): 66.41. HRMS (EI$^+$): 509.2241 [M-I]$^+$. Calcd. for [$C_{26}H_{45}O_2P_2Ni$]: 509.2248. IR (Diamond ATR cell, cm^{-1}): 1624.7 (CO_2), 1372.6, 1359.6, 1320.3.

(*p*-I-^{tBu}PCP)NiH (**5**)

HBPin (28 µL, 0.19 mmol) was added to a flask charged with (*p*-I-^{tBu}PCP)Ni{OC(O)CH$_3$} (100 mg, 0.16 mmol) in benzene (2 mL). The solution changed color from dark golden yellow to bright yellow. After 15 min, the solvent was removed under vacuum to give a yellow residue.

The residue was redissolved in pentane and concentrated, and **5** recrystallized from pentane at -35 °C. Yield: 82 mg (89 %).

^{1}H NMR (C_6D_6, 400.0 MHz): 7.52 (s, 2H, Ar*H*), 3.07 (vt, 4H, ArC*H*$_2$P, J = 3.5 Hz), 1.19 (t, 36H, PC(C*H*$_3$)$_3$, J = 6.4 Hz), -10.12 (t, 1H, Ni*H*, J = 53.0 Hz). ^{13}C{^{1}H} NMR (C_6D_6, 150.8 MHz): 155.1 (t, J = 13.7 Hz), 129.8 (t, J = 8.5 Hz), 90.2 (t, J = 1.6 Hz), 37.5 (t, J = 11.1 Hz), 33.7 (t, J = 8.3 Hz), 29.7 (t, J = 3.0 Hz). ^{31}P{^{1}H} NMR (C_6D_6, 161.9 MHz): 99.92. Anal found (calcd for $C_{24}H_{43}P_2NiI$): C 49.93 (49.77), H 7.28 (7.48) %.

(*p*-I-^{tBu}PCP)Ni{OC(O)H} (**5-CO$_2$**)

(*p*-I-tBuPCP)NiH (**5**) (15 mg, 0.026 mmol) was dissolved in 600 µL C_6D_6 and added to a J Young tube. The nitrogen atmosphere was evacuated, and an excess of 1 atm CO_2 was added via a Schlenk line at room temperature. After 10 min, the solvent was removed to give **5-CO$_2$** as a yellow solid. The product was recrystallized from pentane at -30 °C. Yield: 16 mg (99 %).

^{1}H NMR (C_6D_6, 500.0 MHz): 8.54 (s, 1H, NiOC(O)*H*), 7.03 (s, 2H, Ar*H*), 2.60 (vt, 4H, ArC*H*$_2$P), 1.25 (t, 36H, PC(C*H*$_3$)$_3$, J = 6.5 Hz). ^{13}C{^{1}H} NMR (C_6D_6, 150.8 MHz): 168.4 (s, NiO*C*(O)H), 155.2 (t, J = 12.1 Hz), 130.6 (t, J = 8.2 Hz), 124.8 (s), 90.8 (s), 34.4 (t, J = 6.1 Hz), 32.8 (t, J = 12.4 Hz), 29.5 (t, J = 2.2 Hz). ^{31}P{^{1}H} NMR (C_6D_6, 202.4 MHz): 67.57. IR (Diamond ATR cell, cm^{-1}): 1618.5 (CO_2), 1311.6 (CO_2). Anal found (calcd for $C_{25}H_{43}P_2O_2NiI$): C 48.50 (48.19), H 7.03 (6.96) %.

Titrations of CO_2-Saturated Solvents

CO_2-saturated solvents were prepared by bubbling 1 atm anhydrous CO_2 through the solvent for several hours. In order to quantitatively determine the solubility of CO_2 in each solvent, back-titrations were then performed with 1 N hydrochloric acid using phenolphthalein as the indicator, as initially described by Vianello and co-workers.[7] In a typical titration, a known excess of 1 M aqueous NaOH (10 mL) was added to CO_2-saturated solvent (10 mL). Phenolphthalein was added, and the solution was titrated with 1 N HCl to quantify the [OH^-] that did not react with CO_2. At least four trials were performed with each solvent, and the saturated [CO_2] shown below in Table S1 are the averages of all trials for that particular solvent. Due to difficulties with accurately determining the saturated [CO_2] in diethyl ether using the procedure outlined above, a saturated value of 0.17 M at 25 °C and 1 atm CO_2 was extrapolated from previously reported data[8] and used for all calculations in this paper.

Table S1: Saturated [CO_2] in each solvent as determined by a back-titration with 1 N HCl.

Solvent	Saturated [CO_2] (M)
THF	0.22
Benzene	0.09
1,4-Dioxane	0.28
Acetone	0.25
1,2-Dichloroethane	0.14
1,3-Dimethyl-2-imidazolidinone	0.23
n-Hexane	0.05
Glyme	0.26
Diglyme	0.20
Pyridine	0.18
MeCN	0.26

Stopped-Flow Analysis

All room temperature stopped-flow experiments with **1**, (*p*-OMe-^{tBu}PCP)NiH (**4**), and (*p*-I-^{tBu}PCP)NiH (**5**) were performed using an On-line Instruments Systems, Inc. (Olis) U.S.A. Stopped-Flow paired with an Olis RSM 1000 Rapid Scanning Spectrophotometer. The stopped-flow system was controlled by the Olis Spectral Works Version 4.4 software. All variable temperature stopped-flow experiments with **1** as well as all reactions with **2**, **3**, and **6** were monitored using a TgK Scientific HI-TECH SCIENTIFIC CryoStopped-Flow System (SF-61DX2) apparatus equipped with a diode array detector. The stopped-flow system was controlled by the Kinetic Studio 2.33 software. In a typical experiment, one syringe was loaded with twice the desired concentration of metal hydride (and reaction additive if applicable) in a particular solvent under a dinitrogen atmosphere in a glove box. This was mixed with an equal volume from a second syringe containing twice the desired concentration of CO_2 in the same solvent, loaded under 1 atm of CO_2. The concentration of CO_2 was varied by changing the ratio of CO_2-saturated solvent to blank (stored under N_2) solvent that was loaded into the syringe. Observed rate constants from all stopped-flow experiments were derived using global analysis fitting with the SPECFIT/32 software.[9] All post-run fittings were carried out with the commercial software using non-weighted least square methods. If the initial time (t_0) as defined by the spectrometer did not correspond to t_0 of the reaction (i.e. the spectrometer began collecting data prior to the flow of solution being stopped), the first few scans were discarded and t_0 was manually redefined in the global analysis fitting.

Kinetic Models

The kinetic models used to determine the elementary rate constant k_1 are outlined below.

*i) CO_2 insertion into **1**, **2**, **3**, **4**, or **5** without a LA present*

Kinetic data for CO_2 insertion into the above nickel hydrides were modeled as pseudo-first order reactions, where $[CO_2]$ is ≥20-fold excess to [Ni].

$$A \xrightarrow{k_{obs}} B$$

The second order rate constant k_1 was determined by fitting the data to the rate law k_{obs}[**A**] and then dividing k_{obs} by $[CO_2]$.

*ii) CO_2 insertion into **1** or **2** in the presence of a LA*

As the reaction proceeded in the absence of a LA and varying [LA] (≥20-fold excess with respect to [Ni]) did not change the measured k_{obs} (Table S3), it was concluded that [LA] does not appear in the rate law. Thus, the rate law in the presence of a LA is k_1[**A**]$[CO_2]$ as above, and kinetic data for CO_2 insertion into **1** or **2** in the presence of a LA were modeled as pseudo-first order reactions, where $[CO_2]$ is ≥20-fold excess to [Ni].

$$A \xrightarrow{k_{obs}} B$$

The second order rate constant k_1 was determined by fitting the data to the rate law k_{obs}[**A**] and then dividing k_{obs} by $[CO_2]$.

*iii) CO_2 insertion into **6** without a LA present*

Kinetic data for CO_2 insertion into **6** without a LA present were modeled as mixed second order reactions, where $[\mathbf{6}]_i \neq [CO_2]_i$.

$$A + CO_2 \xrightarrow{k_1} B$$

The second order rate constant k_1 was determined by fitting the data to the rate law k_1[**A**]$[CO_2]$.

*iv) CO_2 insertion into **6** in the presence of a PF_6, OTf, or NTf_2 Salt*

Kinetic data for CO_2 insertion into **6** in the presence of $(^nBu)_4NPF_6$, $LiPF_6$, LiOTf, NaOTf, $NaNTf_2$, $KNTf_2$, or $LiNTf_2$ were modeled as mixed pseudo-second order reactions where $[\mathbf{6}]_i \neq [CO_2]_i \neq$ [LA] and [LA] is ≥20-fold excess to [**6**].

$$A + CO_2 \xrightarrow{k_{obs}} B$$

The third order rate constant k_1 was determined by fitting the data to the rate law k_{obs}[**A**][CO_2] and then dividing k_{obs} by [LA].

*v) CO_2 insertion into **6** in the presence of a BPh_4, $B(C_6F_5)_4$, or $BAr^F{}_4$ Salt*

Due to poor solubility, these reactions could not be performed under pseudo-first order conditions of LA. Kinetic data for CO_2 insertion into **6** in the presence of $LiBPh_4 \cdot 3$ DME, $NaBPh_4$, $KB(C_6F_5)_4$, or $NaBAr^F{}_4$ were modeled as mixed third order reactions where $[\mathbf{6}]_i \neq [CO_2]_i \neq [LA]$.

$$A + CO_2 + LA \xrightarrow{k_1} B + LA$$

The third order rate constant k_1 was determined by fitting the data to the rate law k_1[**A**][CO_2][LA].

Kinetics Traces

Single wavelength kinetic traces were used to check agreement between the data and the chosen kinetic model.

*i) CO_2 insertion into **1***

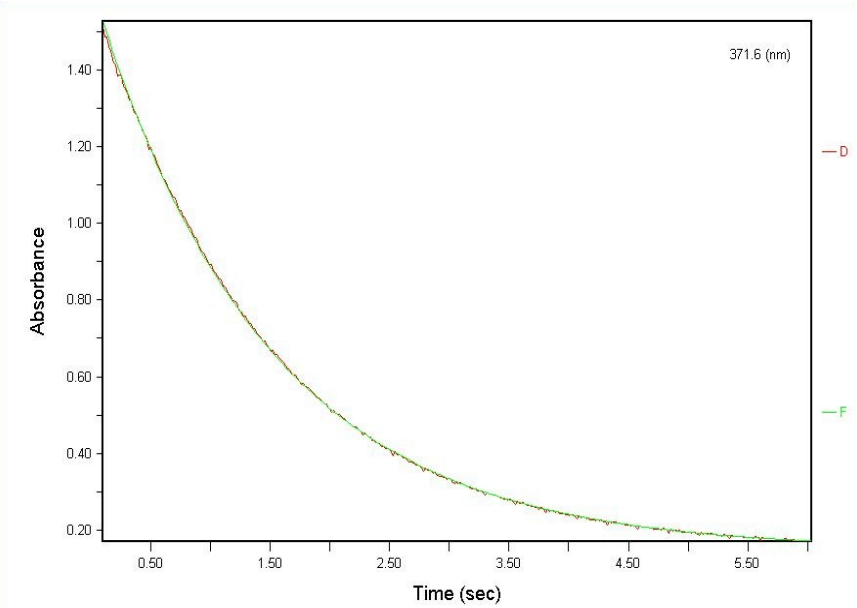

Figure S4: Kinetic trace (371.6 nm) for CO_2 insertion into **1**. Reaction conditions: [**1**] = 0.3 mM, [CO_2] = 45 mM, benzene, room temperature. The data (D) were fit to a pseudo-first order model (F) where [CO_2] is ≥20-fold excess to [**1**].

*ii) CO_2 insertion into **2***

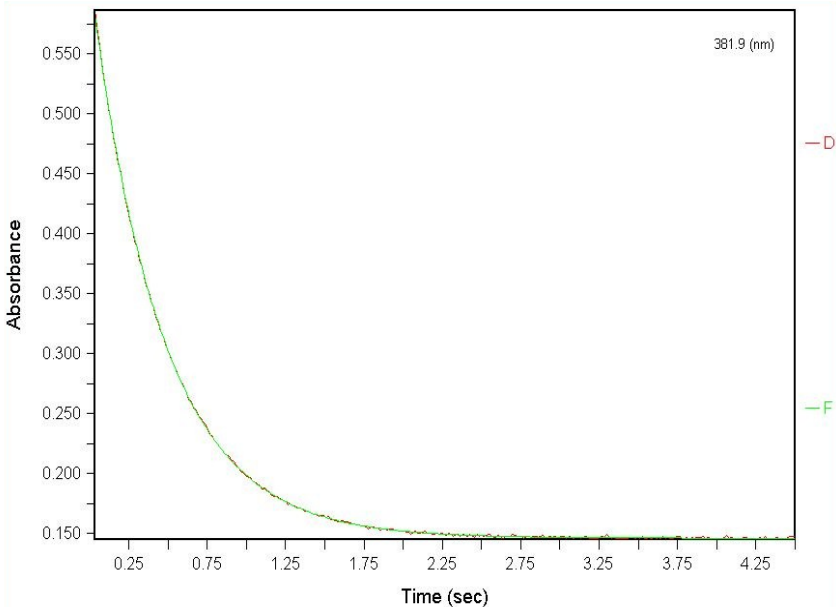

Figure S5: Kinetic trace (381.9 nm) for CO_2 insertion into **2**. Reaction conditions: [**2**] = 0.1 mM, [CO_2] = 4.4 mM, THF, 243 K. The data (D) were fit to a pseudo-first order model (F) where [CO_2] is ≥20-fold excess to [**2**].

*iii) CO_2 insertion into **3***

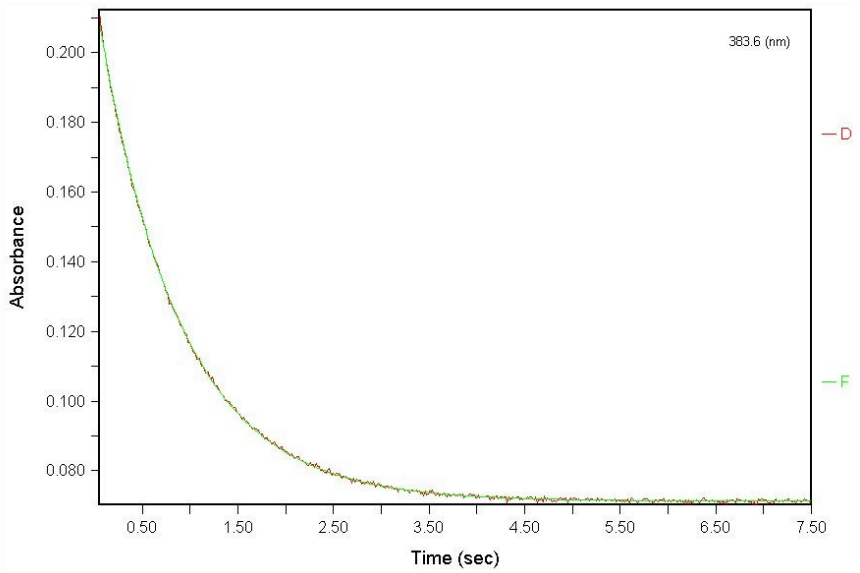

Figure S6: Kinetic trace (383.6 nm) for CO_2 insertion into **3**. Reaction conditions: [**3**] = 0.1 mM, [CO_2] = 2.2 mM, THF, 243 K. The data (D) were fit to a pseudo-first order model (F) where [CO_2] is ≥20-fold excess to [**3**].

*iv) CO_2 insertion into **4***

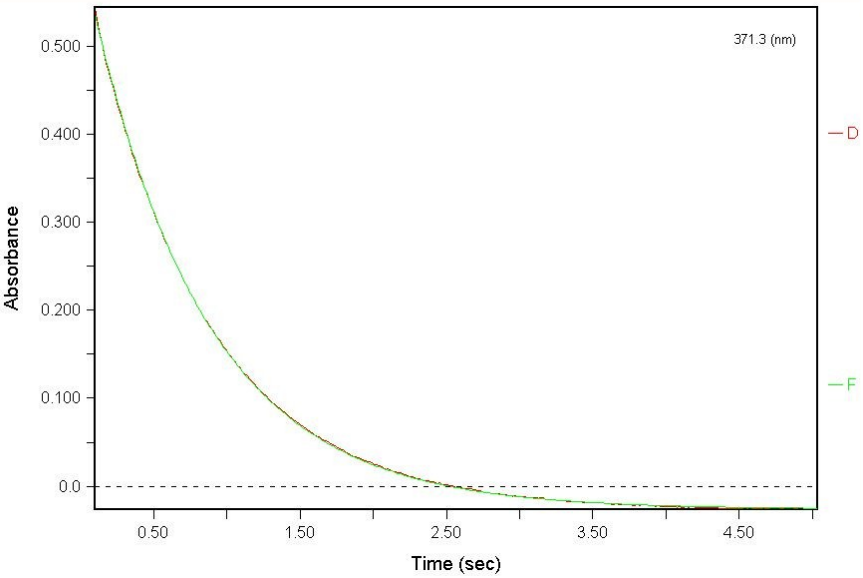

Figure S7: Kinetic trace (371.3 nm) for CO_2 insertion into **4**. Reaction conditions: [**4**] = 0.15 mM, [CO_2] = 110 mM, THF, room temperature. The data (D) were fit to a pseudo-first order model (F) where [CO_2] is ≥20-fold excess to [**4**].

*v) CO_2 insertion into **5***

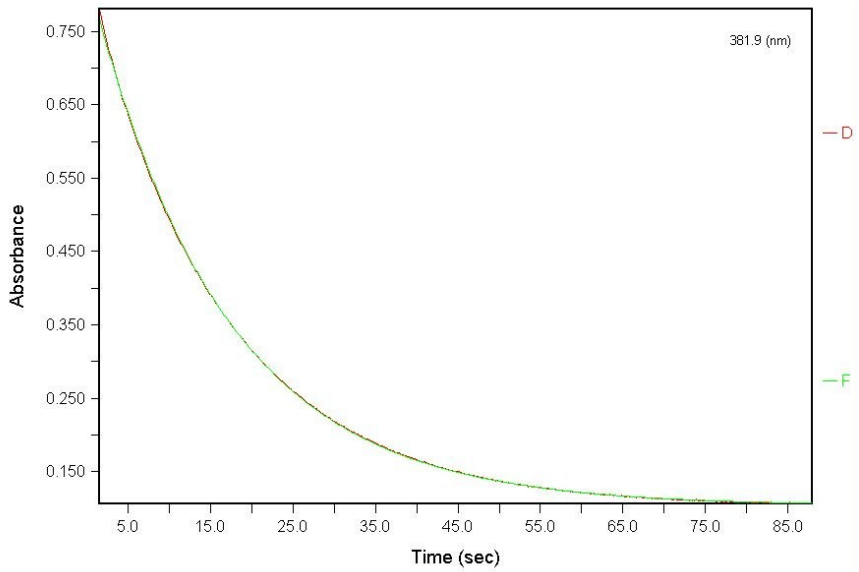

Figure S8: Kinetic trace (381.9 nm) for CO_2 insertion into **5**. Reaction conditions: [**5**] = 0.15 mM, [CO_2] = 44 mM, THF, room temperature. The data (D) were fit to a pseudo-first order model (F) where [CO_2] is ≥20-fold excess to [**5**].

*vi) CO_2 insertion into **6** without a LA present*

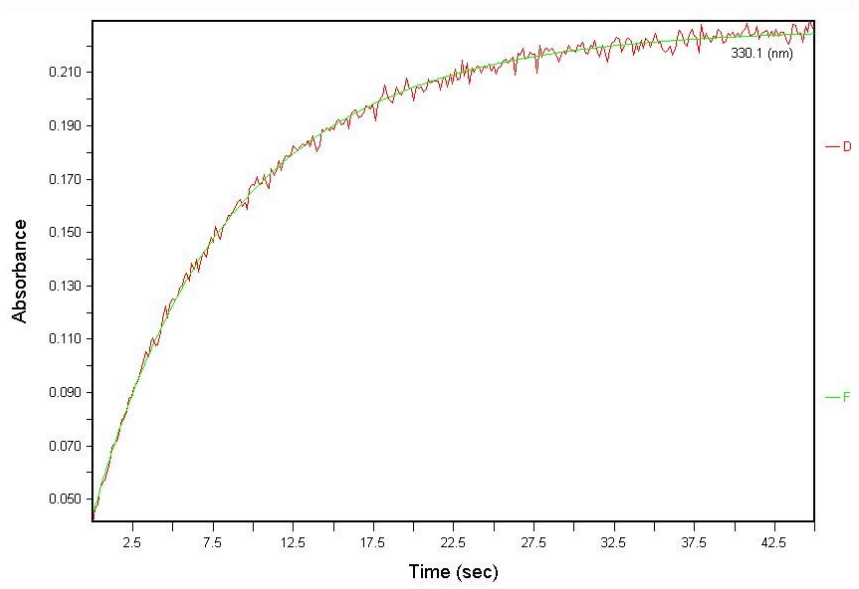

Figure S9: Kinetic trace (330.1 nm) for CO_2 insertion into **6**. Reaction conditions: [**6**] = 2 mM, [CO_2] = 11 mM, THF, 243 K. The data (D) were fit to a mixed second order model (F) where $[\mathbf{6}]_i \neq [CO_2]_i$.

*iii) CO_2 insertion into **6** in the presence of $LiPF_6$*

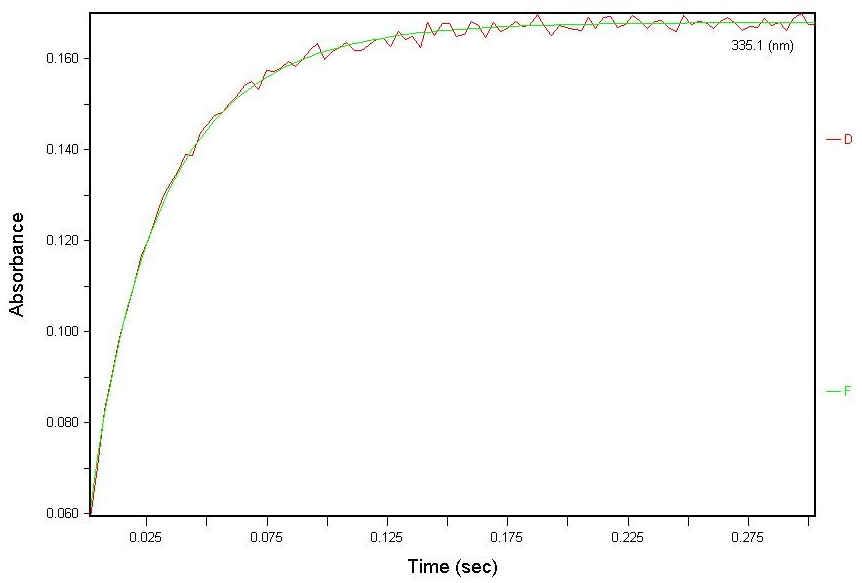

Figure S10: Kinetic trace (335.1 nm) for CO_2 insertion into **6** in the presence of $LiPF_6$. Reaction conditions: [**6**] = 2.25 mM, $[CO_2]$ = 6.6 mM, $[LiPF_6]$ = 0.1125 M, THF, 273 K. The data (D) were fit to a mixed pseudo-second order model (F) where $[\mathbf{6}]_i \neq [CO_2]_i \neq [LiPF_6]_i$ and $[LiPF_6]$ is ≥20-fold excess to [**6**].

Kinetic Order in CO_2

*i) CO_2 insertion into **1***

In order to confirm the reaction order in CO_2, the rate of insertion into **1** was measured under various [CO_2] (≥20-fold excess of CO_2 to [**1**]) in each of the eight solvents tested. The linear relationship between the observed rate constant k_{obs} and [CO_2] confirms that the reaction is first order in CO_2. The slope of the line in each plot is the value of the elementary rate constant k_1 for CO_2 insertion into **1** in that solvent at room temperature.

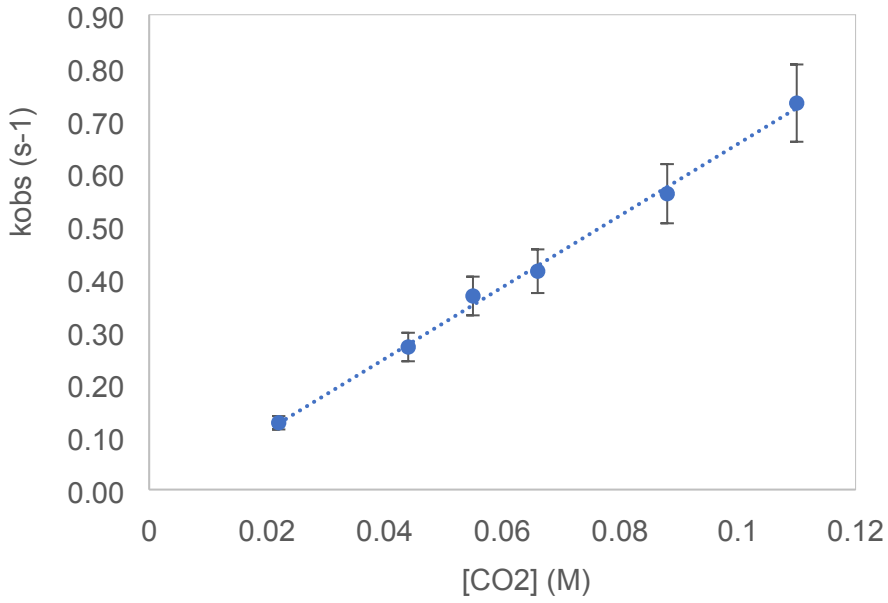

Figure S11: Plot of the observed rate constant (k_{obs}) vs. [CO_2] for CO_2 insertion into **1** in THF. Reaction conditions: [**1**] = 0.30 mM, [CO_2] ranges from 0.022 to 0.11 M, room temperature.

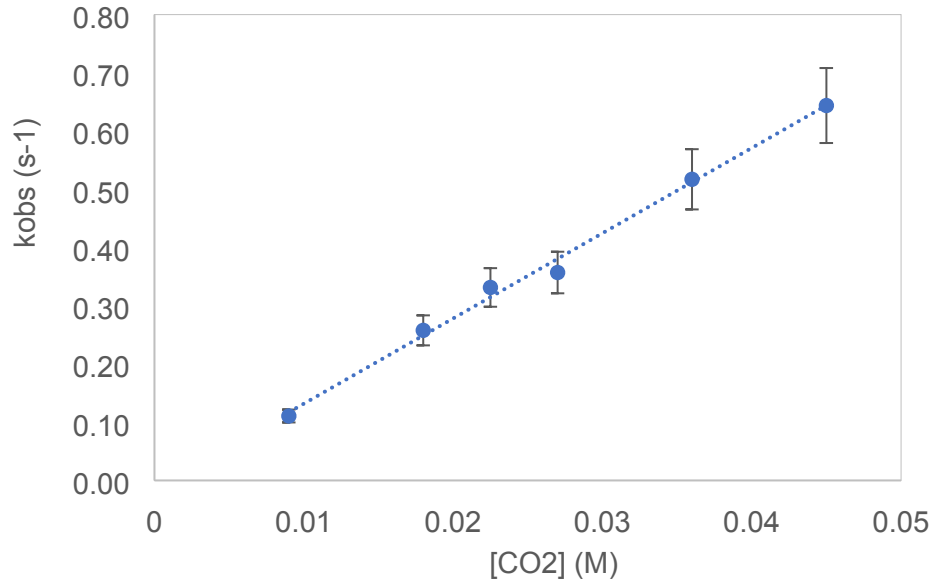

Figure S12: Plot of the observed rate constant (k_{obs}) vs. [CO_2] for CO_2 insertion into **1** in benzene. Reaction conditions: [**1**] = 0.30 mM, [CO_2] ranges from 0.009 to 0.045 M, room temperature.

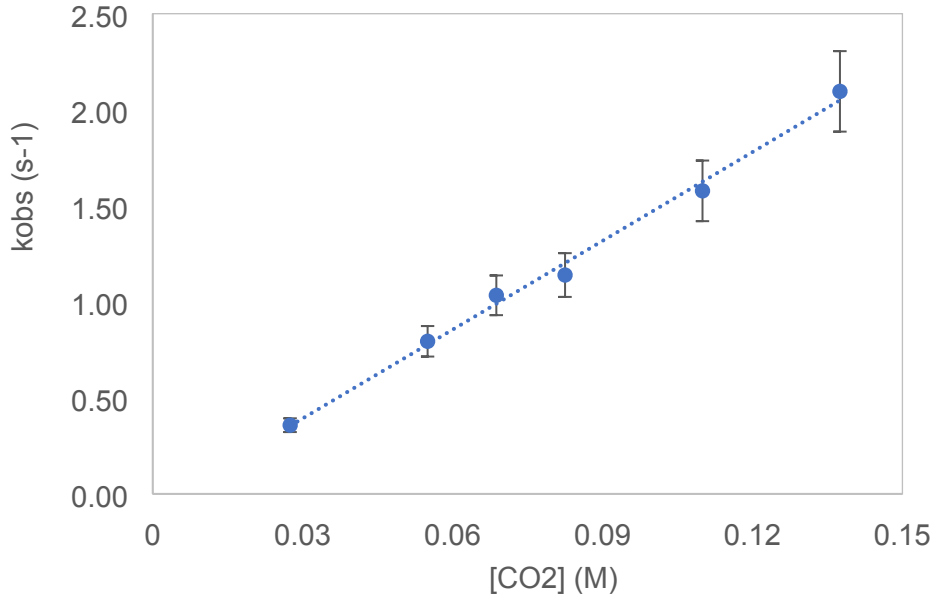

Figure S13: Plot of the observed rate constant (k_{obs}) vs. [CO_2] for CO_2 insertion into **1** in 1,4-dioxane. Reaction conditions: [**1**] = 0.35 mM, [CO_2] ranges from 0.0275 to 0.1375 M, room temperature.

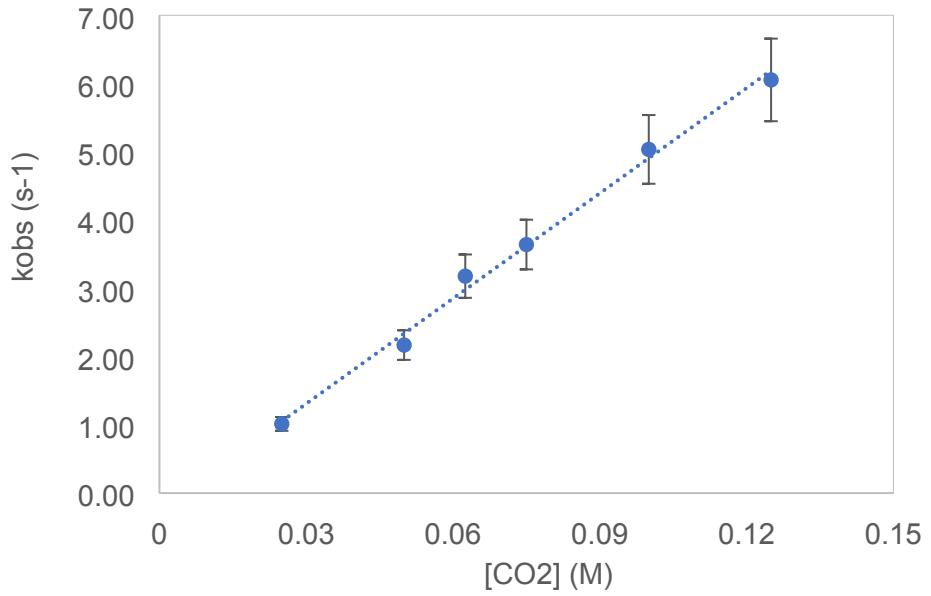

Figure S14: Plot of the observed rate constant (k_{obs}) vs. [CO_2] for CO_2 insertion into **1** in acetone. Reaction conditions: [**1**] = 0.30 mM, [CO_2] ranges from 0.025 to 0.125 M, room temperature.

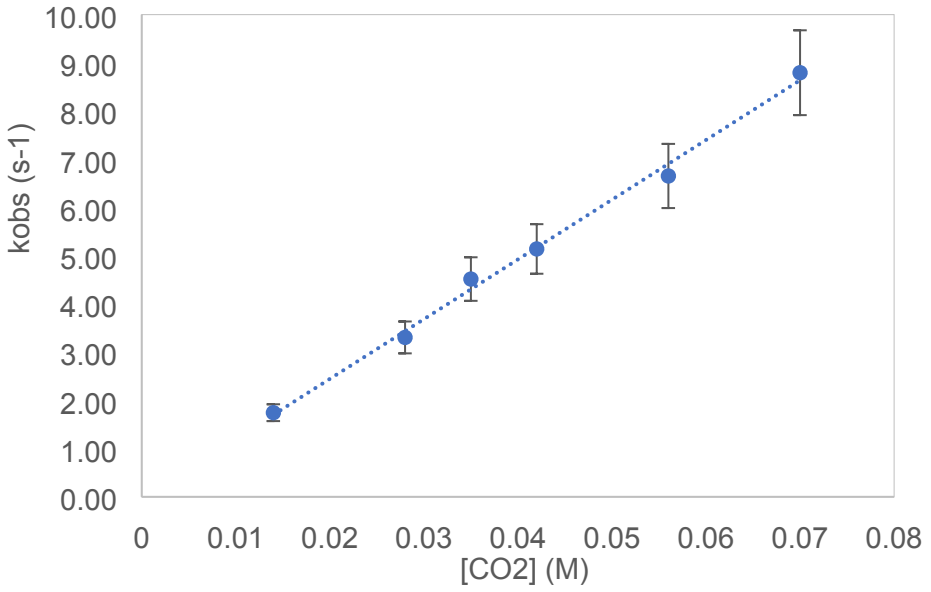

Figure S15: Plot of the observed rate constant (k_{obs}) vs. [CO_2] for CO_2 insertion into **1** in 1,2-dichloroethane. Reaction conditions: [**1**] = 0.30 mM, [CO_2] ranges from 0.014 to 0.07 M, room temperature.

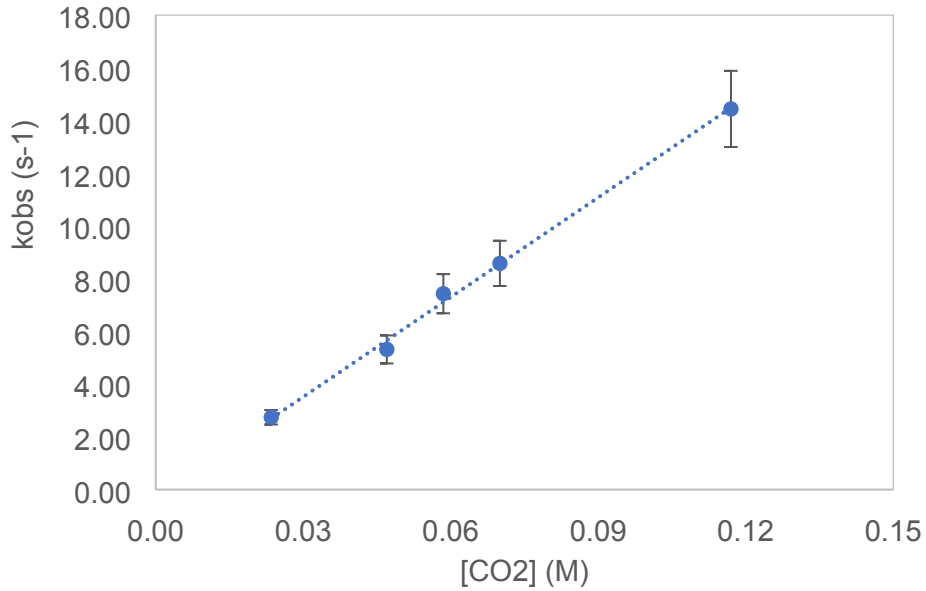

Figure S16: Plot of the observed rate constant (k_{obs}) vs. [CO_2] for CO_2 insertion into **1** in 1,3-dimethyl-2-imidazolidinone. Reaction conditions: [**1**] = 0.35 mM, [CO_2] ranges from 0.0235 to 0.117 M, room temperature.

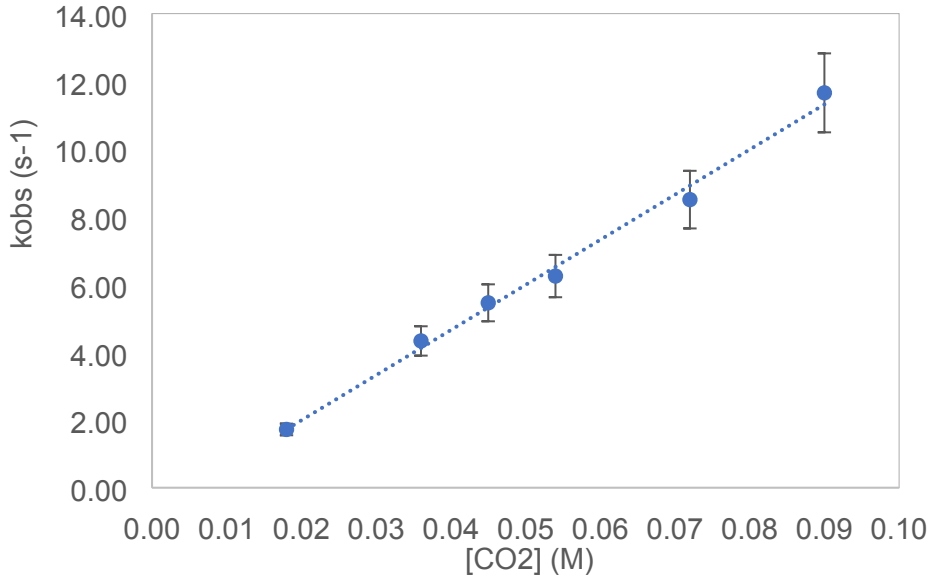

Figure S17: Plot of the observed rate constant (k_{obs}) vs. [CO_2] for CO_2 insertion into **1** in pyridine. Reaction conditions: [**1**] = 0.30 mM, [CO_2] ranges from 0.018 to 0.09 M, room temperature.

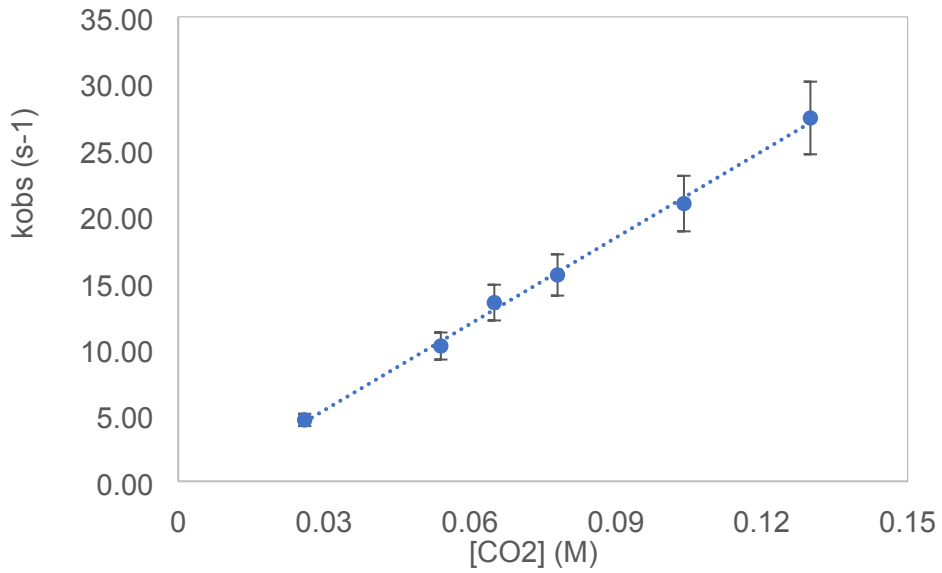

Figure S18: Plot of the observed rate constant (k_{obs}) vs. [CO_2] for CO_2 insertion into **1** in MeCN. Reaction conditions: [**1**] = 0.30 mM, [CO_2] ranges from 0.026 to 0.13 M, room temperature.

*ii) CO_2 insertion into **4***

In order to confirm the reaction order in CO_2, the rate of insertion into **4** was measured under various [CO_2] (≥20-fold excess of CO_2 to [**4**]). The linear relationship between the observed rate constant k_{obs} and [CO_2] confirms that the reaction is first order in CO_2. The slope of the line is the value of the elementary rate constant k_1 for CO_2 insertion into **4** in THF at room temperature.

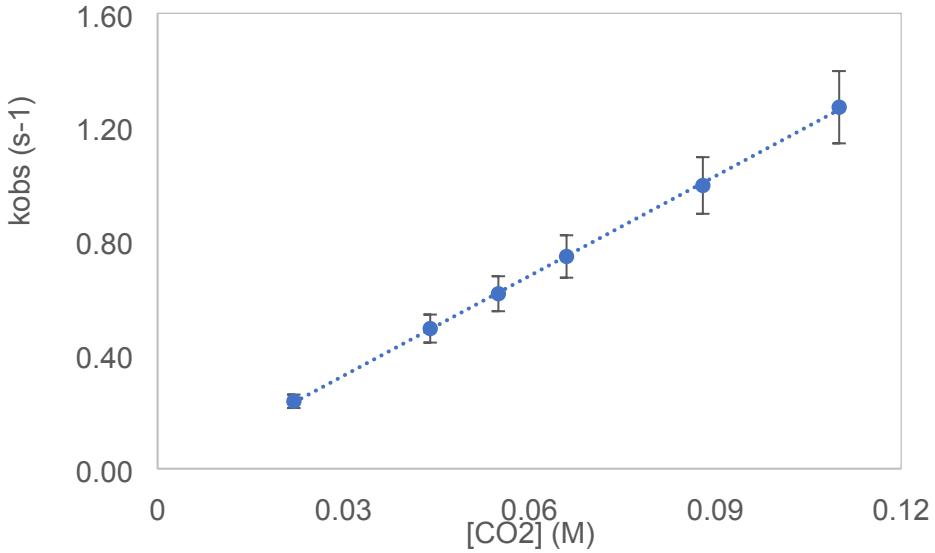

Figure S19: Plot of the observed rate constant (k_{obs}) vs. [CO_2] for CO_2 insertion into **4** in THF. Reaction conditions: [**4**] = 0.15 mM, [CO_2] ranges from 0.022 to 0.11 M, room temperature.

*iii) CO_2 insertion into **5***

In order to confirm the reaction order in CO_2, the rate of insertion into **5** was measured under various [CO_2] (≥20-fold excess of CO_2 to [**5**]). The linear relationship between the observed rate constant k_{obs} and [CO_2] confirms that the reaction is first order in CO_2. The slope of the line is the value of the elementary rate constant k_1 for CO_2 insertion into **5** in THF at room temperature.

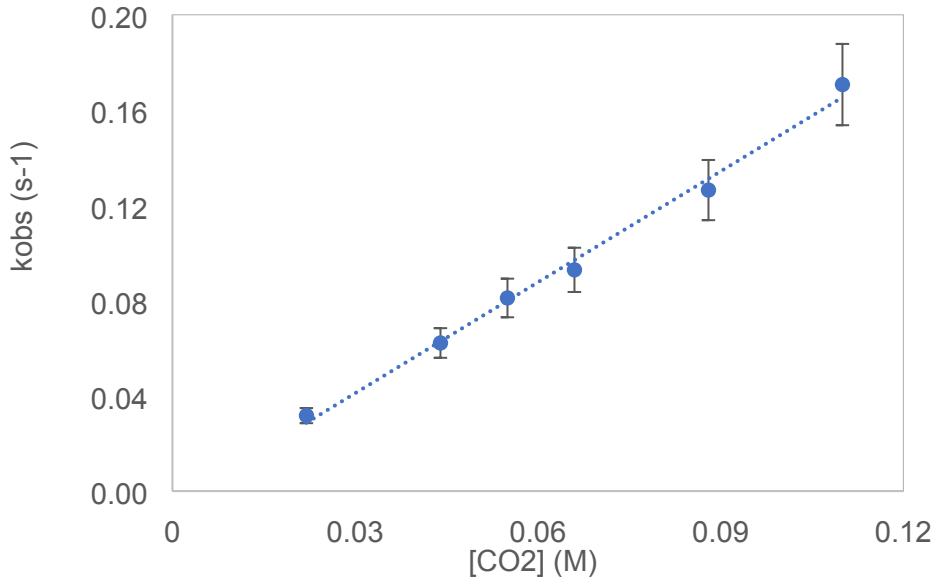

Figure S20: Plot of the observed rate constant (k_{obs}) vs. [CO_2] for CO_2 insertion into **5** in THF. Reaction conditions: [**5**] = 0.15 mM, [CO_2] ranges from 0.022 to 0.11 M, room temperature.

*iv) CO_2 insertion into **6***

In order to confirm the reaction order in CO_2, the rate of insertion into **6** was measured under various [CO_2] in THF. The measured initial rates of insertion at each [CO_2] are given below in Table S2. These values were determined by calculating the slope of the tangent line at t = 0 of the [**6**] vs. time plot. The linear relationship between the measured initial rate ($Rate_i$) and [CO_2] confirms that the reaction is first order in CO_2.

Table S2: The initial rate of CO_2 insertion into **6** measured at each [CO_2].[a]

[CO_2] (M)	$Rate_i$ (M^{-1} s^{-1})
0.0022	3.7×10^{-4}
0.0044	7.0×10^{-4}
0.0066	9.6×10^{-4}
0.0088	1.3×10^{-3}
0.0110	1.5×10^{-3}
0.0132	1.8×10^{-3}

[a]Reaction conditions: [**6**] = 2 mM, THF, 273 K

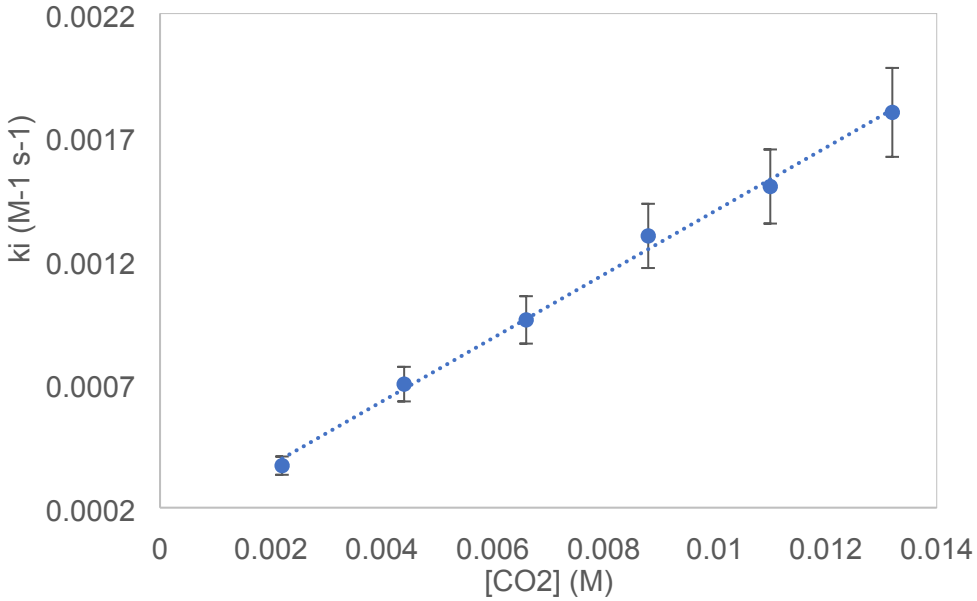

Figure S21: Plot of the measured initial rate ($Rate_i$) vs. [CO_2] for CO_2 insertion into **6** in THF. Reaction conditions: [**6**] = 2 mM, [CO_2] ranges from 0.0022 to 0.0132 M, 273 K.

Kinetic Order in $(^nBu)_4NPF_6$

In order to confirm that there was a first-order dependence on $(^nBu)_4NPF_6$, the rate of CO_2 insertion into **6** was measured in the presence of five different $[(^nBu)_4NPF_6]$ (≥20-fold excess of $(^nBu)_4NPF_6$ to **6**). The linear relationship between the observed rate constant k_{obs} and $[(^nBu)_4NPF_6]$ confirms that the reaction is first order in $(^nBu)_4NPF_6$.

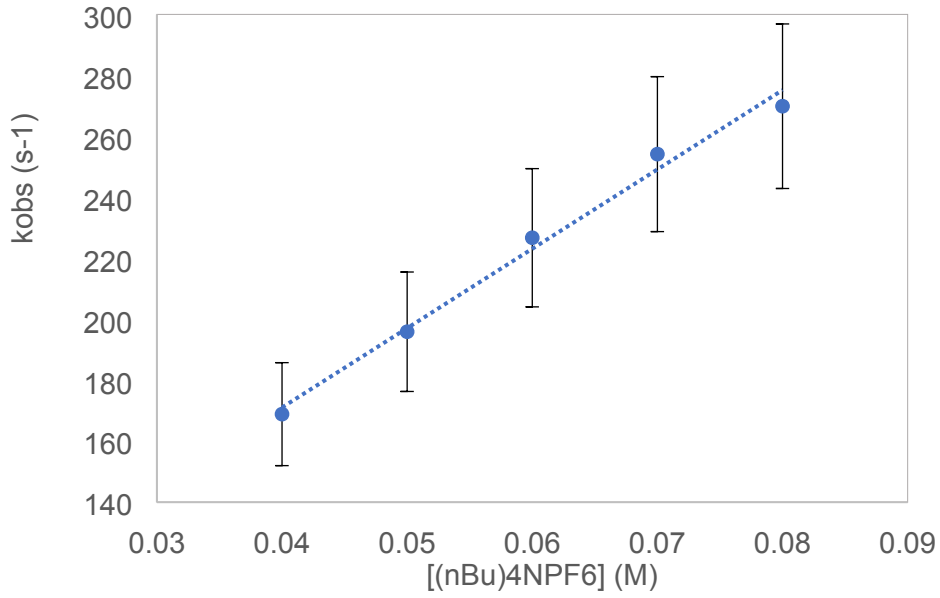

Figure S22: Plot of the observed rate constant (k_{obs}) vs. $[(^nBu)_4NPF_6]$ for CO_2 insertion into **6**. Reaction conditions: [**6**] = 2 mM, $[CO_2]$ = 4.4 mM, $[(^nBu)_4NPF_6]$ = 40-80 mM, THF, 273 K.

Lewis Acid Studies with (^{tBu}PCP)NiH (1)

The rate of CO_2 insertion into **1** was measured in the presence of both ionic and non-ionic Lewis acids. The solvent was also varied. No rate enhancement was seen under any set of conditions.

Table S3: Screen for LA effect on CO_2 insertion into **1**.

Solvent	[**1**] (mM)	[CO_2] (M)	Lewis Acid	[LA] (mM)	k_{obs} (s^{-1}) at RT	k_1 (M^{-1} s^{-1}) at RT
THF	0.3	0.11	None	-	0.74	6.7 ± 0.67
THF	0.3	0.11	$LiPF_6$	6	0.73	6.6 ± 0.66
THF	0.3	0.11	$LiPF_6$	30	0.74	6.7 ± 0.67
THF	0.3	0.11	$NaBAr^F{}_4$ [a]	6	0.74	6.7 ± 0.67
MeCN	0.3	0.13	None	-	25.5	196 ± 19.6
MeCN	0.3	0.13	$LiPF_6$	6	25.6	197 ± 19.7
MeCN	0.3	0.13	$LiPF_6$	30	26.7	205 ± 20.5
MeCN	0.3	0.13	$LiPF_6$	240	-	-
Benzene	0.3	0.045	None	-	0.53	11.7 ± 1.17
Benzene	0.3	0.045	BPh_3	6	0.54	12.1 ± 1.21
Benzene	0.3	0.045	BPh_3	30	0.53	11.8 ± 1.18

[a]$NaBAr^F{}_4$ = sodium tetrakis[3,5-bis(trifluoromethyl)phenyl]borate.

Plots of Solvent Parameters vs. ln(k_1) for CO_2 Insertion into 1 and 6

*i) Plot of dielectric constant vs. ln(k_1) for CO_2 insertion into **1***

The values of ln(k_1) for CO_2 insertion into **1** in various solvents were plotted against the corresponding solvent dielectric constants ε.

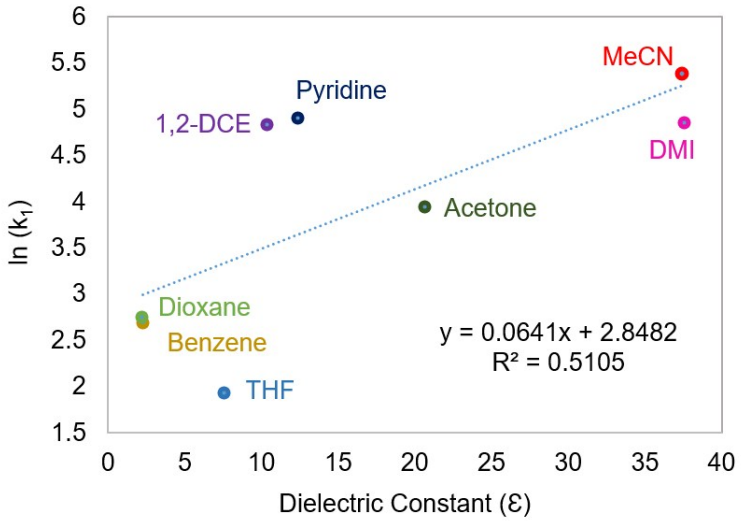

Figure S23: Relationship between the second-order rate constant k_1 for CO_2 insertion into **1** in various solvents and the dielectric constant of the solvent.

ii) Plot of dielectric constant vs. ln(k_1) for CO_2 insertion into ***6***

The values of ln(k_1) for CO_2 insertion into **6** in the seven solvents measured were plotted against the corresponding solvent dielectric constants ε.

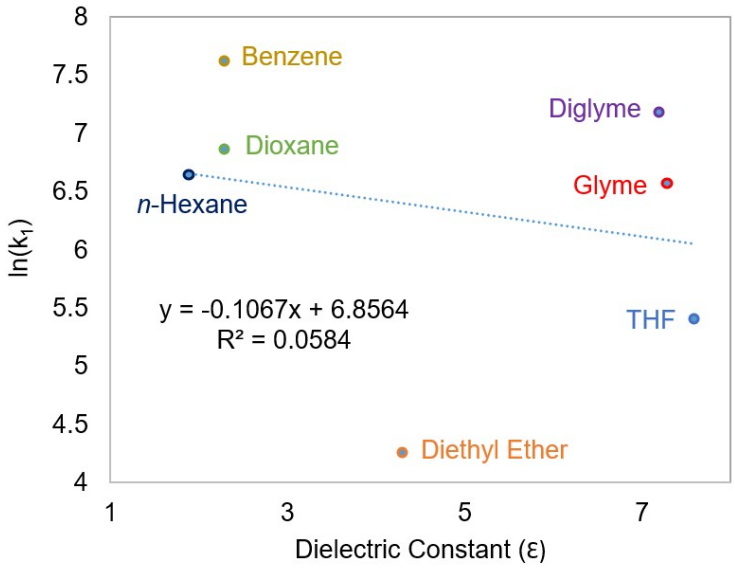

Figure S24: Relationship between the second-order rate constant k_1 for CO_2 insertion into **6** in all seven solvents tested and the dielectric constant of the solvent.

iii) Plot of acceptor number vs. ln(k_1) for CO_2 insertion into ***6***

The values of ln(k_1) for CO_2 insertion into **6** in the seven solvents measured were plotted against the corresponding solvent acceptor number.

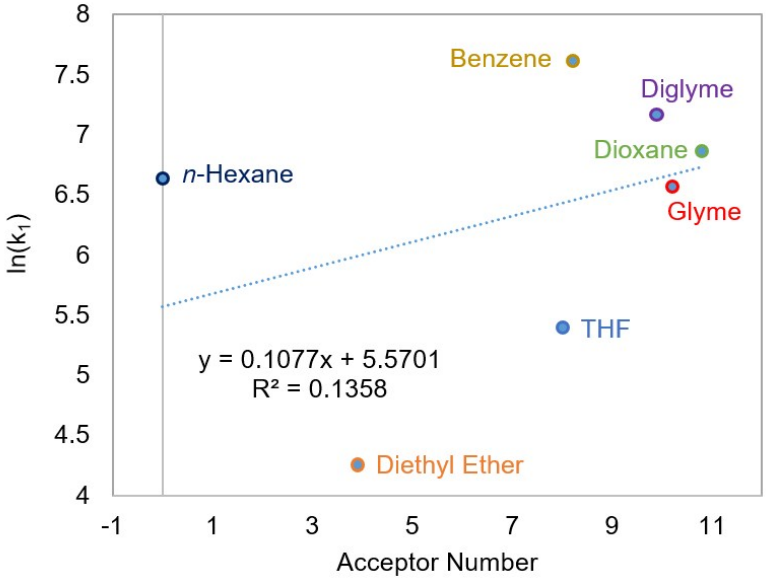

Figure S25: Relationship between the second-order rate constant k_1 for CO_2 insertion into **6** in all seven solvents tested and the acceptor number of the solvent.

Calculated Rates of Product Formation for CO_2 Insertion into 6

In order to compare rates independent of molecularity, the rates of product formation in M s^{-1} were calculated from the measured k_1 values (Table 6) under the following conditions: [**6**] = 2 mM, [CO_2] = 4.4 mM; [Additive] = 40 mM, THF, 273 K.

For Entry 1:

Rate of Product Formation (M s^{-1}) = k_1[**6**][CO_2] = k_1[0.002 M][0.0044 M]

For Entries 2-12:

Rate of Product Formation (M s^{-1}) = k_1[**6**][CO_2][LA] = k_1[0.002 M][0.0044 M][0.04 M]

Table S4: Rates of product formation for CO_2 insertion into **6**.

Entry	Additive	Measured k_1[a]	Rate of Product Formation (M s^{-1})	Rate Increase
1	None	64 ± 6	5.6 (6) x 10^{-4}	-
2	$(^nBu)_4NPF_6$	4.0 (4) x 10^3	1.4 (1) x 10^{-3}	3
3	LiOTf	1.5 (2) x 10^4	5.3 (5) x 10^{-3}	9
4	NaOTf	2.4 (2) x 10^4	8.4 (8) x 10^{-3}	15
5	$NaNTf_2$	3.0 (3) x 10^4	1.1 (1) x 10^{-2}	19
6	$KNTf_2$	4.0 (4) x 10^4	1.4 (1) x 10^{-2}	25
7	$LiPF_6$	4.9 (5) x 10^4	1.7 (2) x 10^{-2}	30
8	$LiNTf_2$	7.3 (7) x 10^4	2.6 (3) x 10^{-2}	46
9	$LiBPh_4 \cdot 3$ DME	1.2 (1) x 10^5	4.2 (4) x 10^{-2}	72
10	$NaBPh_4$	1.3 (1) x 10^5	4.6 (5) x 10^{-2}	82
11[f]	$KB(C_6F_5)_4$	1.4 (1) x 10^5	4.9 (5) x 10^{-2}	88
12[f]	$NaBAr^F{}_4$	1.6 (2) x 10^5	5.6 (6) x 10^{-2}	100

[a] k_1 in M^{-1} s^{-1} for Entry 1 and M^{-2} s^{-1} for Entries 2-12.

Eyring Plots

Eyring plots were constructed to determine $\Delta S^{\ddagger}$ and $\Delta H^{\ddagger}$ for the insertion of CO_2 into **1**, **2**, **3**, and **6** under a range of conditions. $\Delta G^{\ddagger}$ was calculated from $\Delta G^{\ddagger} = \Delta H^{\ddagger} - T\Delta S^{\ddagger}$ (See Tables 1, 3, 5 and 6 for determined activation parameters).

*i) CO_2 insertion into **1***

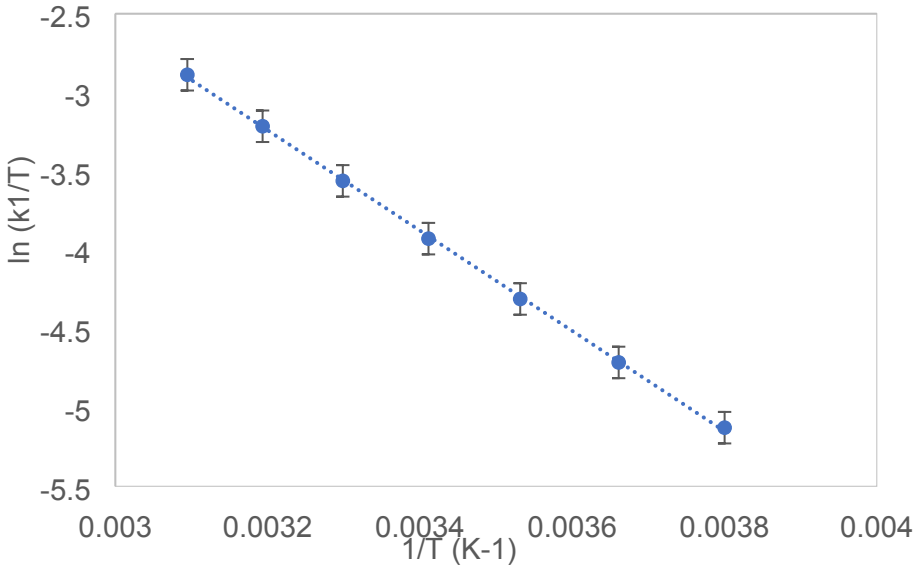

Figure S26: Eyring plot of CO_2 insertion into **1** in THF. Reaction conditions: [**1**] = 0.3 mM, [CO_2] = 0.11 M, temperature ranges from -10 to 50 °C in 10 °C increments. The k_1 values used here are the second order rate constants from k_1[**1**][CO_2].

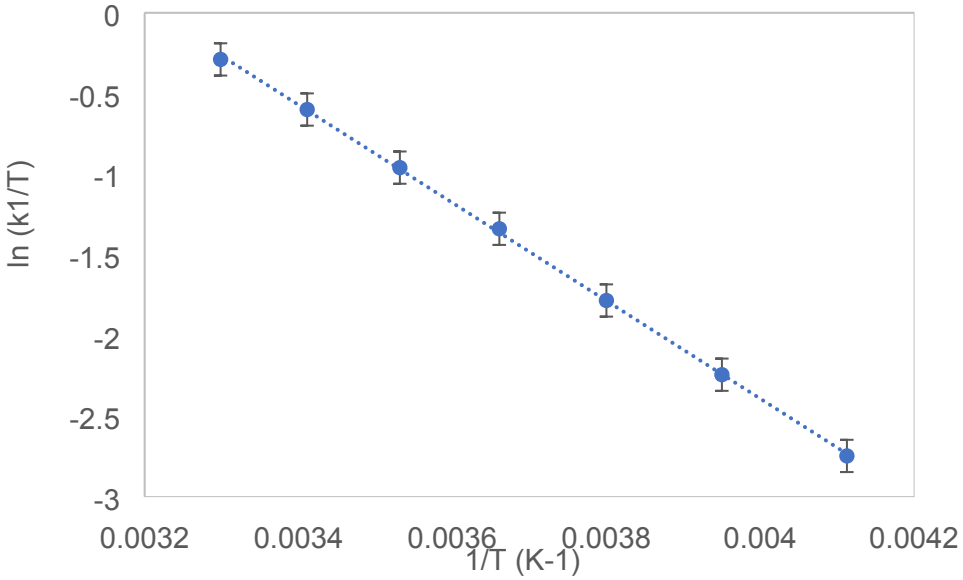

Figure S27: Eyring plot of CO_2 insertion into **1** in MeCN. Reaction conditions: [**1**] = 0.4 mM, [CO_2] = 0.065 M, temperature ranges from -30 to 30 °C in 10 °C increments. The k_1 values used here are the second order rate constants from k_1[**1**][CO_2].

*ii) CO_2 insertion into **2***

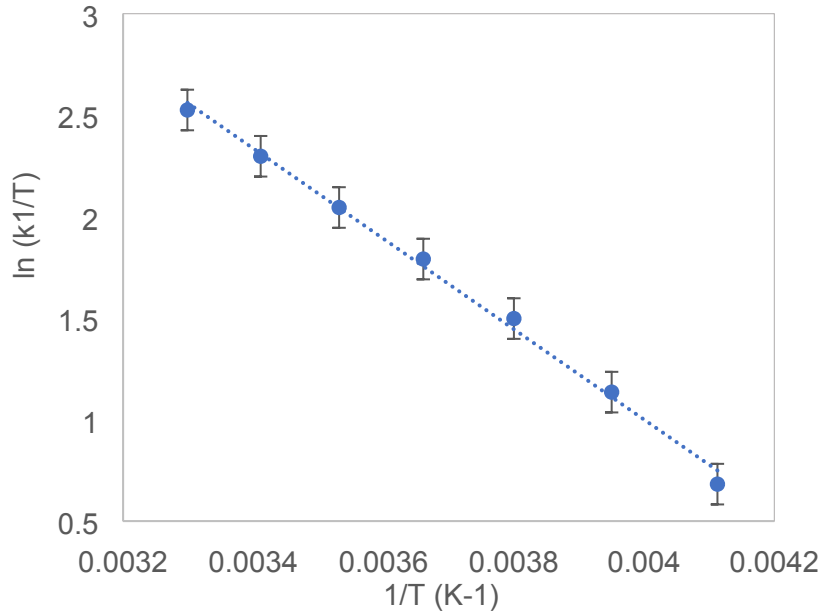

Figure S28: Eyring plot of CO_2 insertion into **2** in THF. Reaction conditions: [**2**] = 0.1 mM, [CO_2] = 4.4 mM, temperature ranges from -30 to 30 °C in 10 °C increments. The k_1 values used here are the second order rate constants from k_1[**2**][CO_2].

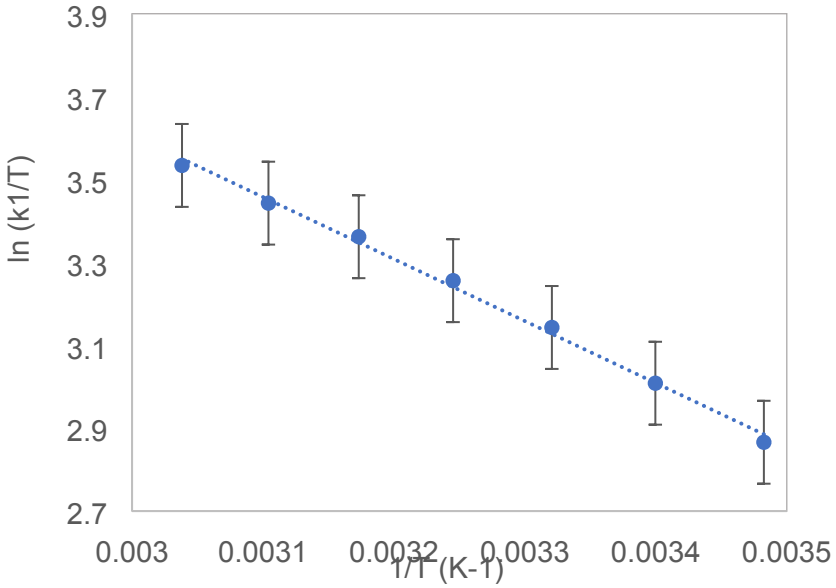

Figure S29: Eyring plot of CO_2 insertion into **2** in benzene. Reaction conditions: [**2**] = 0.1 mM, [CO_2] = 2.7 mM, temperature ranges from 14 to 56 °C in 7 °C increments. The k_1 values used here are the second order rate constants from k_1[**2**][CO_2].

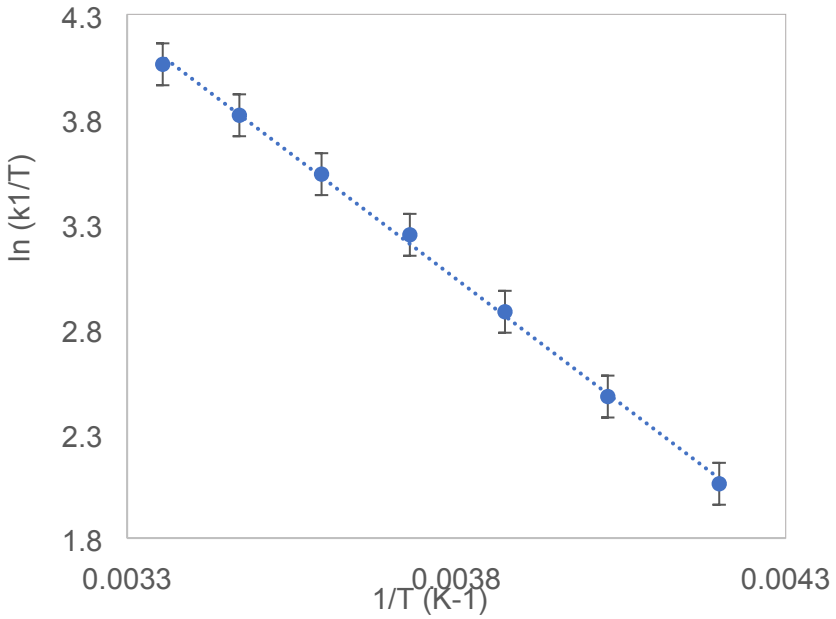

Figure S30: Eyring plot of CO_2 insertion into **2** in pyridine. Reaction conditions: [**2**] = 0.1 mM, [CO_2] = 3.6 mM, temperature ranges from -35 to 25 °C in 10 °C increments. The k_1 values used here are the second order rate constants from k_1[**2**][CO_2].

*iii) CO_2 insertion into **3***

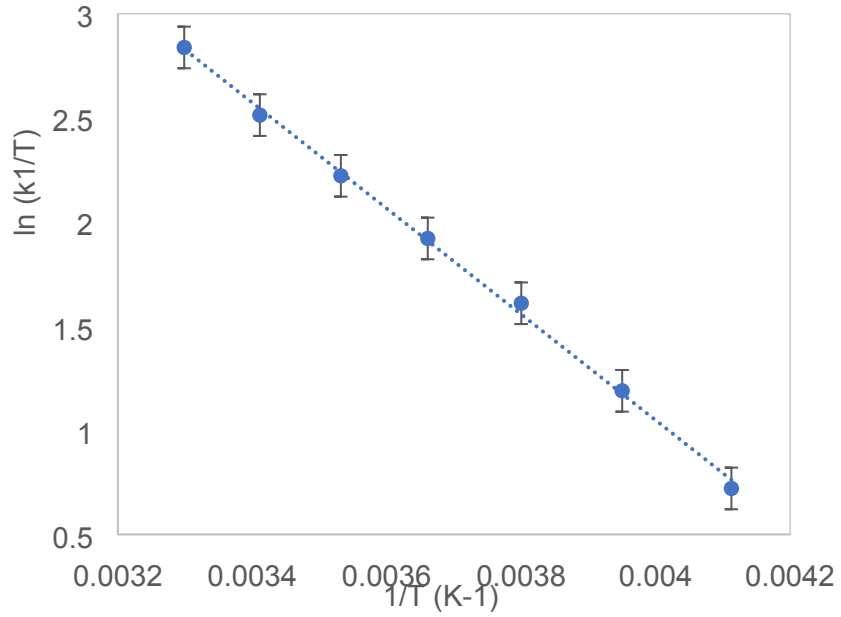

Figure S31: Eyring plot of CO_2 insertion into **3** in THF. Reaction conditions: [**3**] = 0.1 mM, [CO_2] = 2.2 mM, temperature ranges from -30 to 30 °C in 10 °C increments. The k_1 values used here are the second order rate constants from k_1[**3**][CO_2].

*iv) CO_2 insertion into **6** without a LA present*

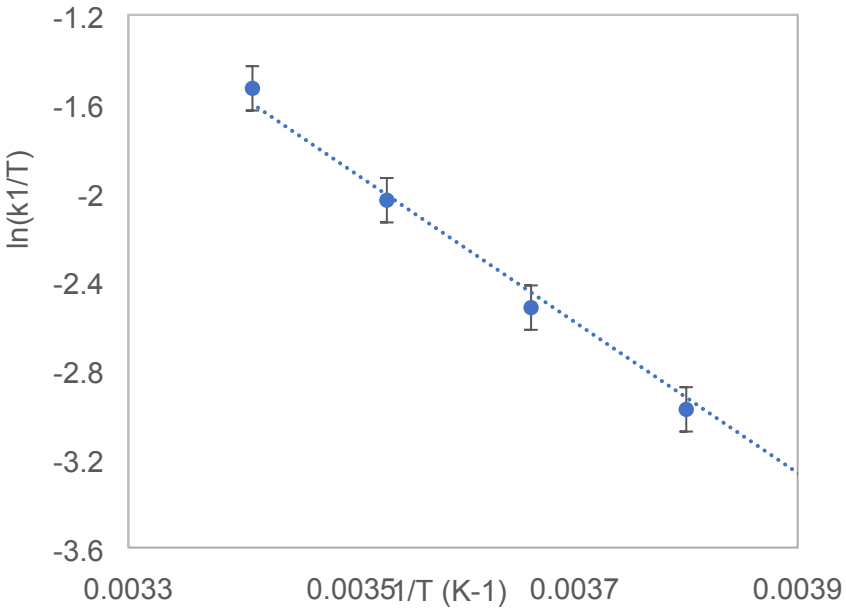

Figure S32: Eyring plot of CO_2 insertion into **6** in diethyl ether. Reaction conditions: [**6**] = 2 mM, [CO_2] = 34 mM, temperature ranges from -20 to 20 °C in 10 °C increments. The k_1 values used here are the second order rate constants from k_1[**6**][CO_2].

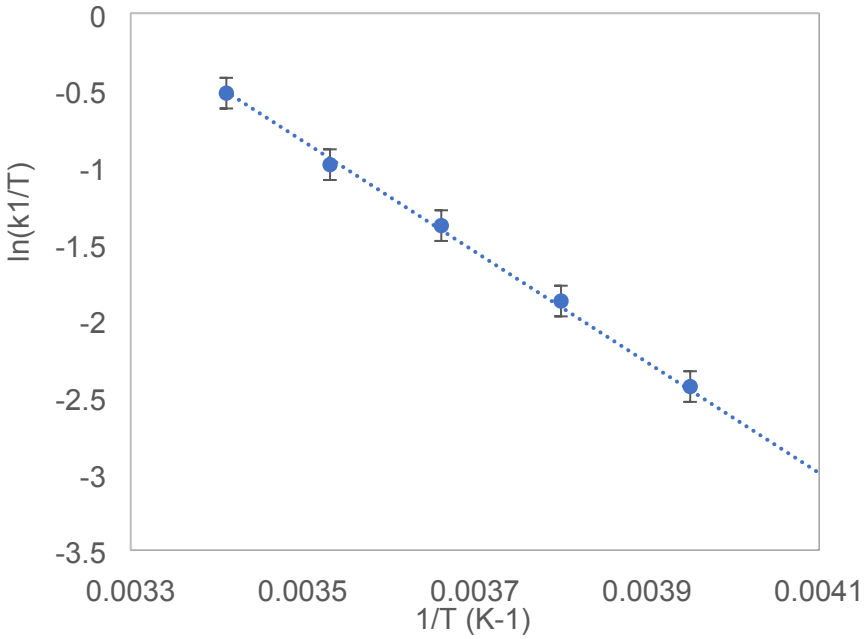

Figure S33: Eyring plot of CO_2 insertion into **6** in THF. Reaction conditions: [**6**] = 2 mM, [CO_2] = 11 mM, temperature ranges from -30 to 20 °C in 10 °C increments. The k_1 values used here are the second order rate constants from k_1[**6**][CO_2].

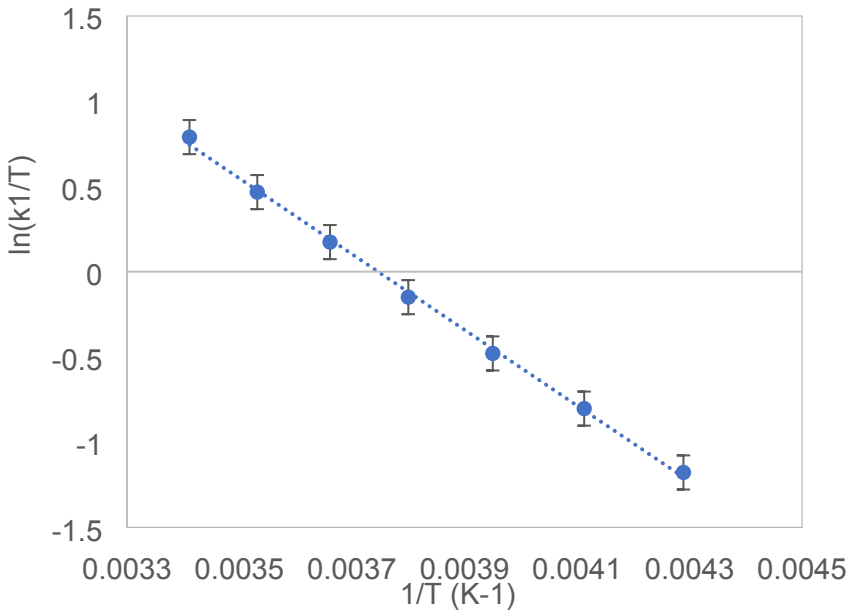

Figure S34: Eyring plot of CO_2 insertion into **6** in glyme. Reaction conditions: [**6**] = 2 mM, [CO_2] = 10 mM, temperature ranges from -40 to 20 °C in 10 °C increments. The k_1 values used here are the second order rate constants from k_1[**6**][CO_2].

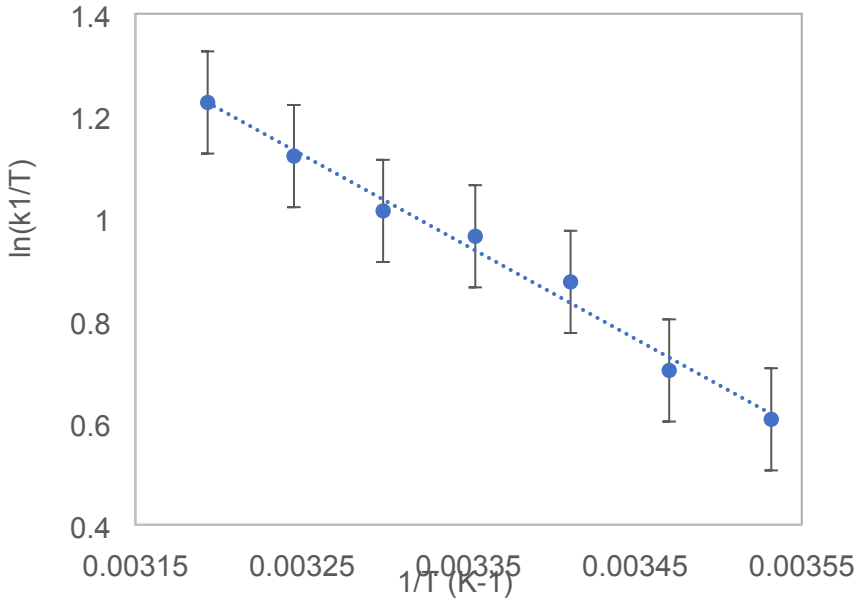

Figure S35: Eyring plot of CO_2 insertion into **6** in *n*-hexane. Reaction conditions: [**6**] = 2 mM, [CO_2] = 6 mM, temperature ranges from 10 to 40 °C in 5 °C increments. The k_1 values used here are the second order rate constants from k_1[**6**][CO_2].

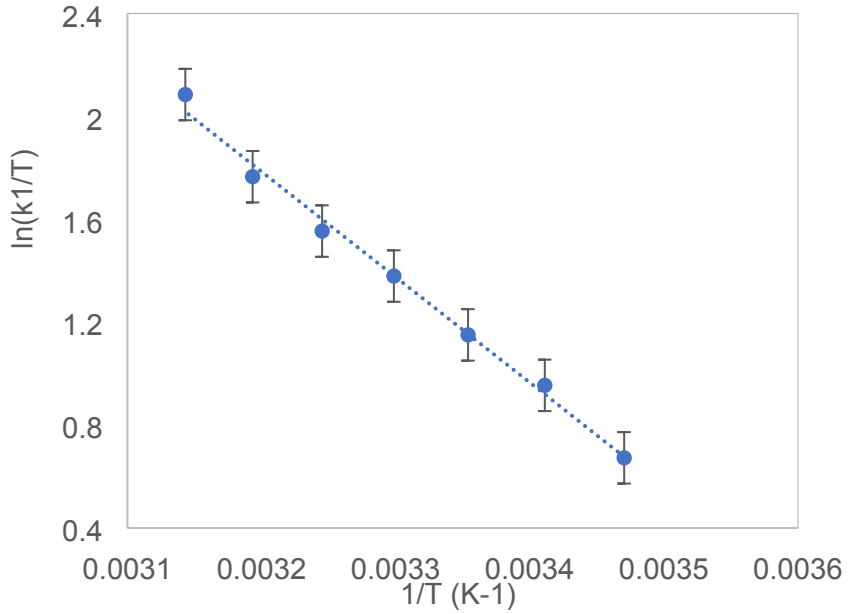

Figure S36: Eyring plot of CO_2 insertion into **6** in 1,4-dioxane. Reaction conditions: [**6**] = 2 mM, [CO_2] = 2.8 mM, temperature ranges from 15 to 45 °C in 5 °C increments. The k_1 values used here are the second order rate constants from k_1[**6**][CO_2].

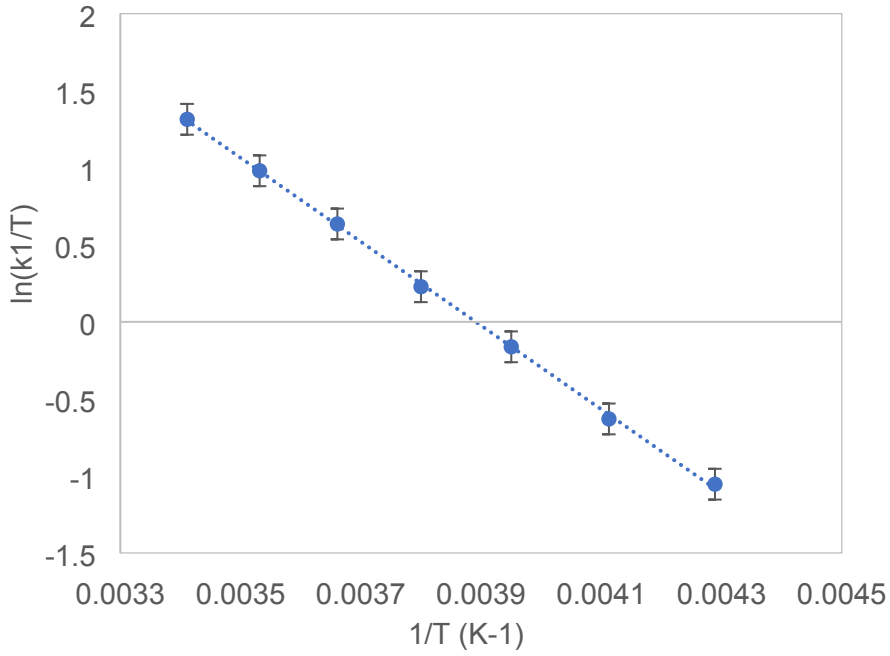

Figure S37: Eyring plot of CO_2 insertion into **6** in diglyme. Reaction conditions: [**6**] = 2 mM, [CO_2] = 10 mM, temperature ranges from -40 to 20 °C in 10 °C increments. The k_1 values used here are the second order rate constants from k_1[**6**][CO_2].

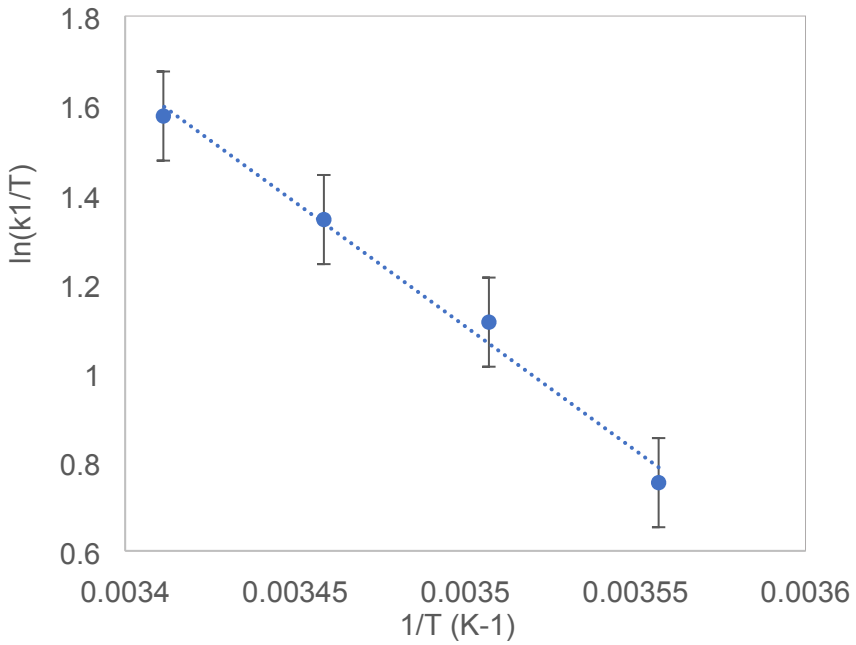

Figure S38: Eyring plot of CO_2 insertion into **6** in benzene. Reaction conditions: [**6**] = 2 mM, [CO_2] = 3.6 mM, temperature ranges from 8 to 20 °C in 4 °C increments. The k_1 values used here are the second order rate constants from k_1[**6**][CO_2].

*v) CO_2 insertion into **6** in the presence of an additive*

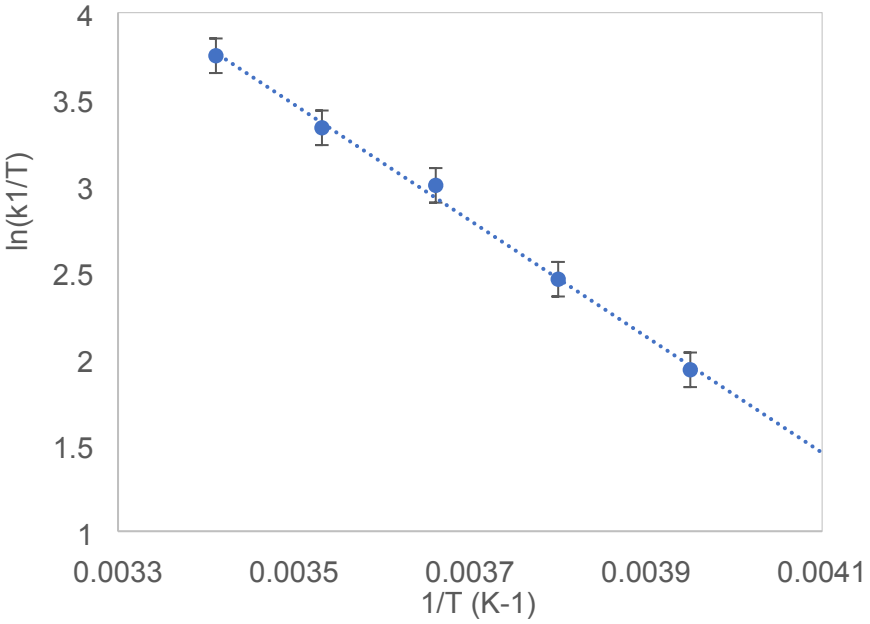

Figure S39: Eyring plot of CO_2 insertion into **6** in the presence of $(^nBu)_4NPF_6$ in THF. Reaction conditions: [**6**] = 2 mM, [CO_2] = 4.4 mM, [$(^nBu)_4NPF_6$] = 0.04 M, temperature ranges from -30 to 20 °C in 10 °C increments. The k_1 values used here are the third order rate constants from k_1[**6**][CO_2][$(^nBu)_4NPF_6$].

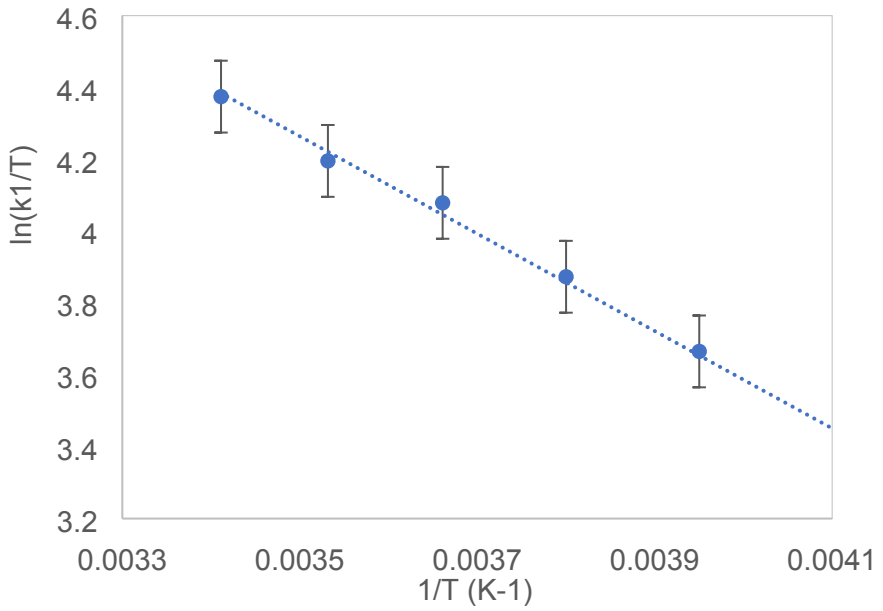

Figure S40: Eyring plot of CO_2 insertion into **6** in the presence of LiOTf in THF. Reaction conditions: [**6**] = 2 mM, [CO_2] = 4.4 mM, [LiOTf] = 0.04 M, temperature ranges from -30 to 20 °C in 10 °C increments. The k_1 values used here are the third order rate constants from k_1[**6**][CO_2][LiOTf].

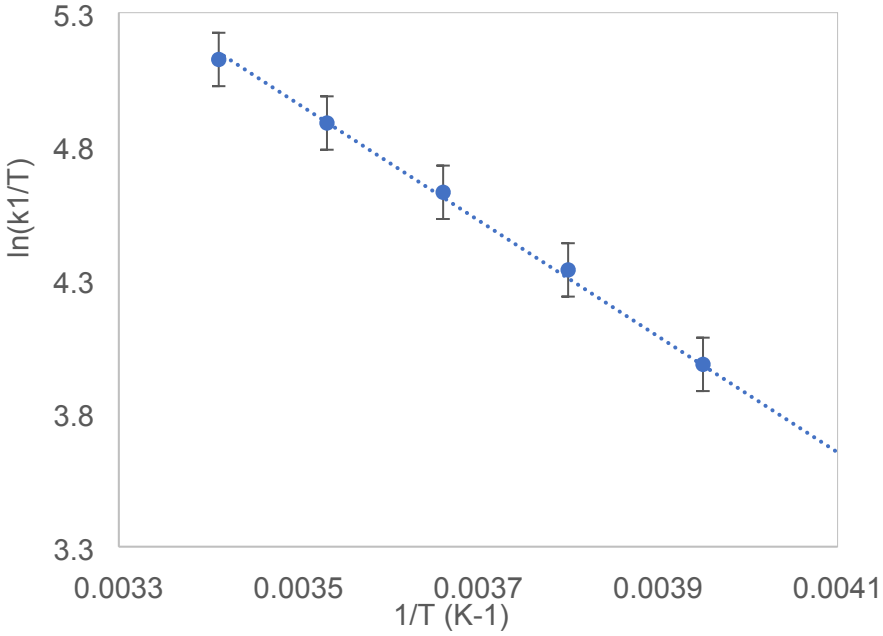

Figure S41: Eyring plot of CO_2 insertion into **6** in the presence of NaOTf in THF. Reaction conditions: [**6**] = 2 mM, [CO_2] = 4.4 mM, [NaOTf] = 0.04 M, temperature ranges from -30 to 20 °C in 10 °C increments. The k_1 values used here are the third order rate constants from k_1[**6**][CO_2][NaOTf].

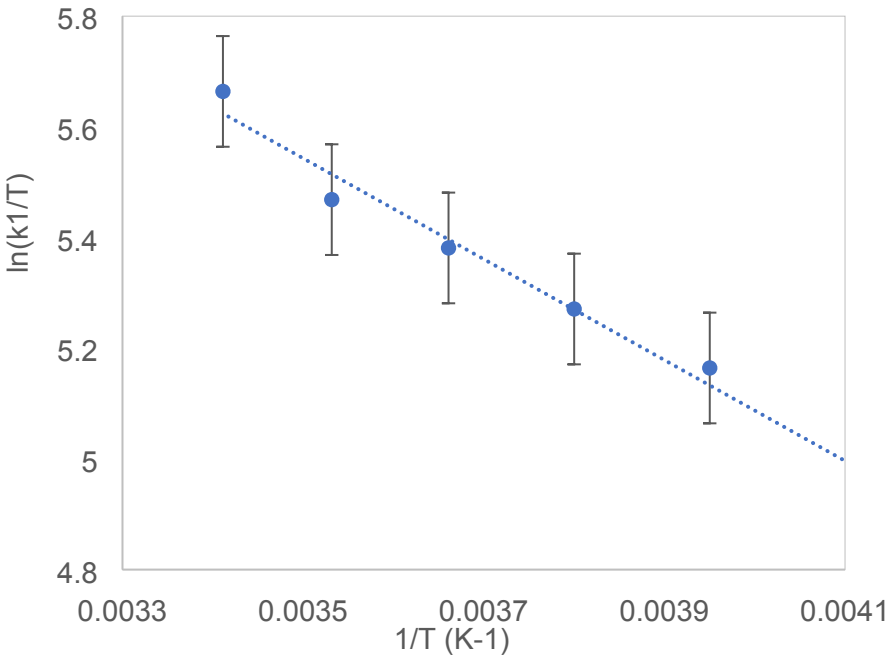

Figure S42: Eyring plot of CO_2 insertion into **6** in the presence of $LiPF_6$ in THF. Reaction conditions: [**6**] = 2 mM, [CO_2] = 4.4 mM, [$LiPF_6$] = 0.04 M, temperature ranges from -30 to 20 °C in 10 °C increments. The k_1 values used here are the third order rate constants from k_1[**6**][CO_2][$LiPF_6$].

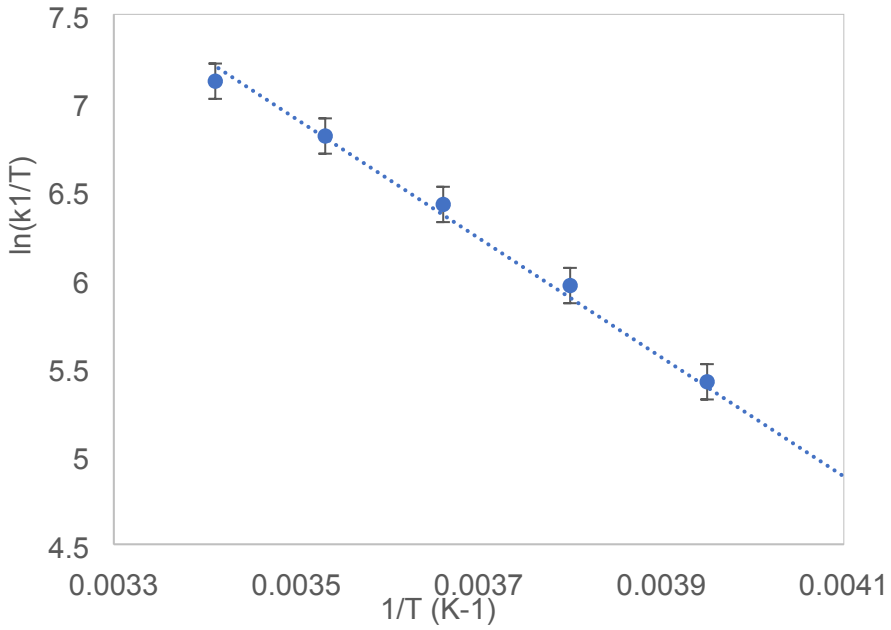

Figure S43: Eyring plot of CO_2 insertion into **6** in the presence of $NaBAr^F_4$ in THF. Reaction conditions: [**6**] = 2 mM, [CO_2] = 2.2 mM, [$NaBAr^F_4$] = 0.02 M, temperature ranges from -30 to 20 °C in 10 °C increments. The k_1 values used here are the third order rate constants from k_1[**6**][CO_2][$NaBAr^F_4$].

Kinetic Isotope Effect

i) Synthesis of (^{tBu}PCP)NiD

(^{tBu}PCP)NiD was synthesized by a modification of the literature procedure.[1] (^{tBu}PCP)NiCl (80 mg) and $NaBD_4$ (60 mg) were dissolved in a 1:1 mixture of C_6H_6 and CH_3CH_2OD (15 mL). The solution was stirred overnight. 200 mg $NaBD_4$ was then added, and the solution was stirred for an additional 3 h. The solvent was removed under vacuum and the product extracted into benzene (10 mL) and filtered. The solvent was again removed under vacuum and pentane added. The desired metal deuteride was crystallized from pentane as yellow needles.

ii) Calculating KIE

As the sample of (^{tBu}PCP)NiD contained protio impurity, ^{1}H NMR spectroscopy was used to determine the % hydride in each sample of deuteride synthesized.

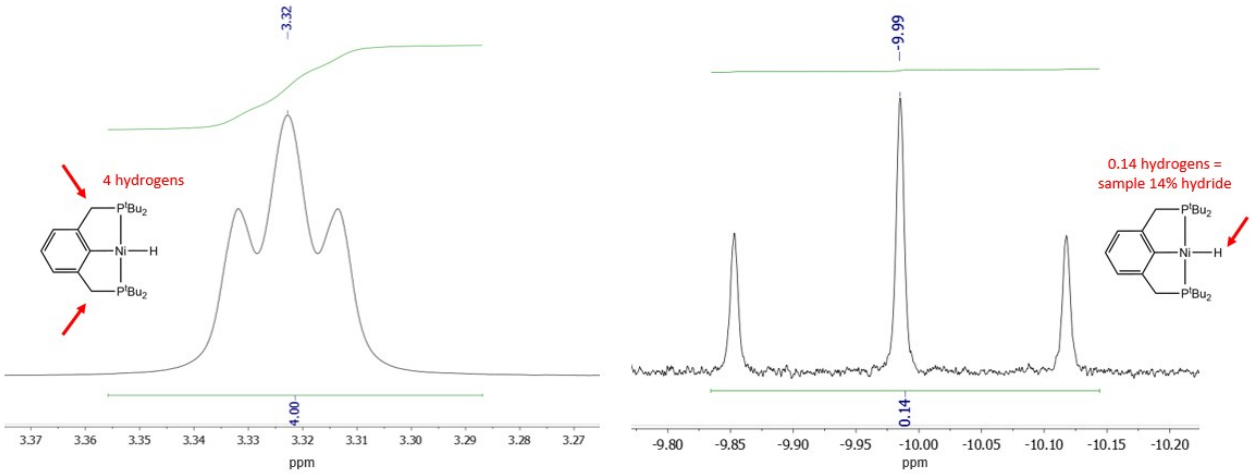

Figure S44: Selected sections of ^{1}H NMR spectrum of (^{tBu}PCP)NiD showing the presence of (^{tBu}PCP)NiH. The % hydride was determined by comparing the integral of a known chemical environment (here the signal of the four Ar*CH*$_2$ protons at 3.32 ppm) with that of the hydride signal at -10.0 ppm. This spectrum was taken in C_6D_6 and with a relaxation time of 10 sec.

When calculating the KIE, the measured k_{obs} for the deuteride at each [CO_2] was corrected for the amount of metal hydride present. Specifically, the measured k_{obs} was taken as the linear combination $k_{obs} = Hk_{Hobs} + Dk_{Dobs}$, where H is the % hydride, k_{Hobs} is the observed rate of CO_2 insertion into the metal hydride at a given [CO_2], D is the % deuteride, and k_{Dobs} is the observed rate of CO_2 insertion into the metal deuteride at the same [CO_2]. Based on the known values of k_{obs}, H, k_H, and D, it was possible to solve for k_{Dobs} for each [CO_2].

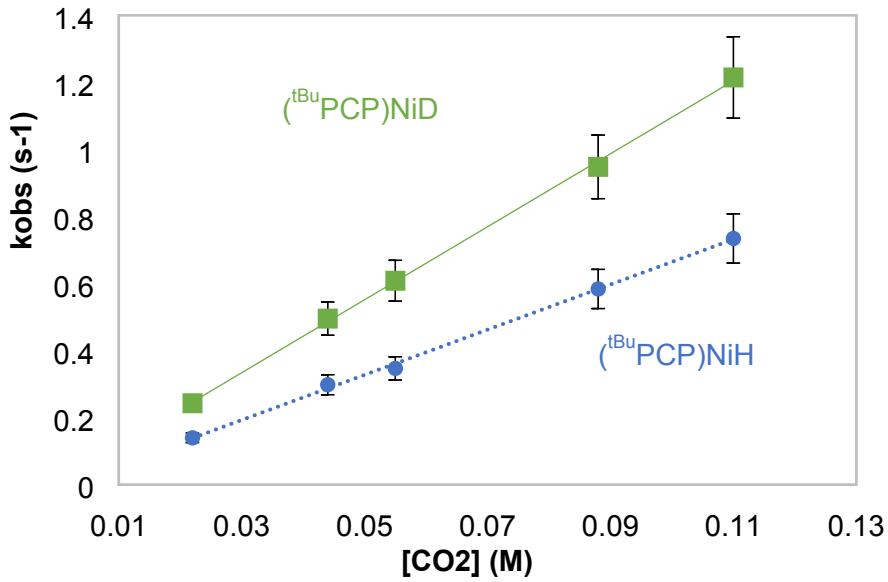

Figure S45: Plot of the observed rate constants (k_{obs}) vs. [CO_2] for CO_2 insertion into **1** and (^{tBu}PCP)NiD in THF. The values of k_{obs} plotted for the insertion into (^{tBu}PCP)NiD have been corrected as explained above. Reaction conditions: [**1**] = 0.30 mM, [(^{tBu}PCP)NiD] = 0.30 mM, [CO_2] ranges from 0.022 to 0.11 M, room temperature.

$$KIE\ in\ THF = \frac{k_H}{k_D} = \frac{6.7}{11} = 0.61$$

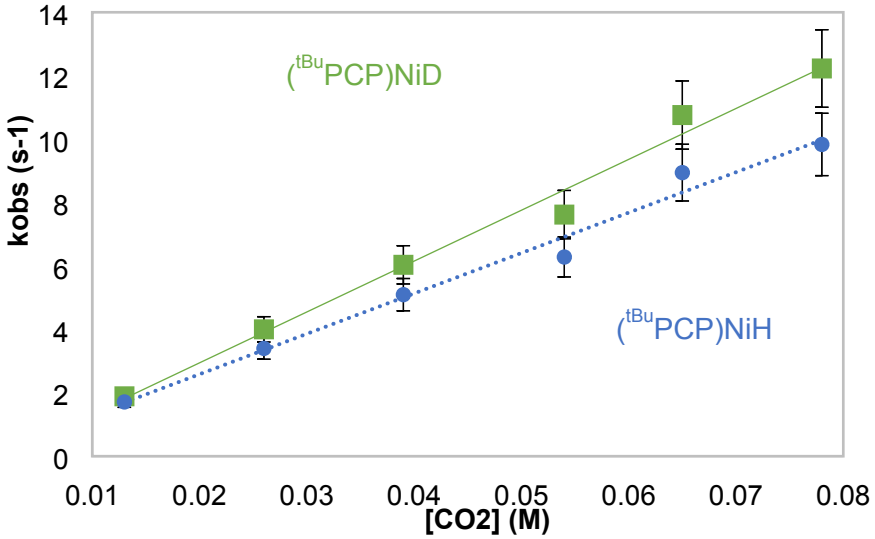

Figure S46: Plot of the observed rate constants (k_{obs}) vs. [CO_2] for CO_2 insertion into **1** and (^{tBu}PCP)NiD in MeCN. The values of k_{obs} plotted for the insertion into (^{tBu}PCP)NiD have been corrected as explained above. Reaction conditions: [**1**] = 0.30 mM, [(^{tBu}PCP)NiD] = 0.30 mM, [CO_2] ranges from 0.013 to 0.078 M, room temperature.

$$KIE\ in\ MeCN = \frac{k_H}{k_D} = \frac{127}{160} = 0.79$$

References

1. B. J. Boro, E. N. Duesler, K. I. Goldberg and R. A. Kemp, *Inorg. Chem.*, 2009, **48**, 5081-5087.
2. K. Krogh-Jespersen, M. Czerw, K. Zhu, B. Singh, M. Kanzelberger, N. Darji, P. D. Achord, K. B. Renkema and A. S. Goldman, *J. Am. Chem. Soc.*, 2002, **124**, 10797-10809.
3. Z. E. Clarke, P. T. Maragh, T. P. Dasgupta, D. G. Gusev, A. J. Lough and K. Abdur-Rashid, *Organometallics*, 2006, **25**, 4113-4117.
4. E. Hollink, J. C. Stewart, P. Wei and D. W. Stephan, *Dalton Trans.*, 2003, 3968-3974.
5. D. Alberico, A. Rudolph and M. Lautens, *J. Org. Chem.*, 2007, **72**, 775-781.
6. T. J. Schmeier, N. Hazari, C. D. Incarvito and J. A. Raskatov, *Chem. Commun.*, 2011, **47**, 1824-1826.
7. A. Gennaro, A. A. Isse and E. Vianello, *J. Electroanal. Chem.*, 1990, **289**, 203-215.
8. A. Christoff, *Z. Phys. Chem.*, 1912, **79**, 456.
9. R. A. Binstead, B. Jung and A. D. Zuberbühler, Spectrum Software Associates: Marlborough, MA 01752 (USA).